Lateral variation of crust and upper mantle structures in NW Iran derived from surface wave analysis

G. Mortezanejad · H. Rahimi · F. Romanelli · G. F. Panza

Abstract To obtain the shear velocity structure across North-West of Iran and surrounding areas to a depth of 160 km, we performed a namely Hedgehog nonlinear inversion on Rayleigh wave group velocity dispersion curves in the period range from 7 to 60 s. The distributed dispersion curves are the results of our surface wave dispersion tomography using the data of 280 local and regional seismic events, recorded by the medium- and broad-band seismic stations in the region. We outline different crust and upper mantle structures for the study area based on calculated group and shear velocities. Our results reveal relatively low velocities at the shorter periods (7–10 s) in the presence of sedimentary basins (e.g., South Caspian Basin) and for eastern Anatolia and relatively high velocities along the Sanandaj–Sirjan Metamorphic zone, Alborz, Talesh, and the Lesser Caucasus Mountains. By depth inversion of group velocities, we observed 14-km-thick sediments in South Caspian Basin and Kura Depression. Based on our maps at 20 s, we outline different crustal models for the region and highlight the differences between South Caspian Basin and NW Iran, on one side, and the similarities between the South Caspian Basin and Kura Depression that extend beneath Talesh, Alborz, and Lesser Caucasus, on the other. Comparing the shear velocity of lower crust in South Caspian Basin and Kura Depression with that of NW Iran proves different origination of lower crust in the basin, probably oceanic source, because of its significant higher shear velocity rather than NW Iran. In Talesh, we observe indications of an under-thrusting of the lower crust of SCB beneath NW Iran while the middle crust is locked. The analysis of group velocities at longer periods (≥ 35 s) and obtained shear velocity models allows us to outline different lithospheric structures and crustal depth in the region. The high group velocities in Talesh, South Caspian Sea, and Lesser Caucasus on one side and Zagros Folding and Thrust Belt on the other, beside the result of shear velocity models, suggest the presence of a stable and thick mantle lid that seems to be thin or absent in the eastern Anatolia and much of NW Iran. The shallowest Moho

G. Mortezanejad · H. Rahimi (✉)
Institute of Geophysics, University of Tehran, North Kargar St, Tehran, Iran
e-mail: rahimih@ut.ac.ir

F. Romanelli
Department of Mathematics and Geosciences, University of Trieste, via E. Weiss 4, 34127 Trieste, Italy

G. F. Panza
Accademia Nazionale dei Lincei, Rome, Italy

G. F. Panza
Institute of Geophysics, China Earthquake Administration, Beijing, China

G. F. Panza
International Seismic Safety Organization (ISSO), Arsita, Italy
http://www.issoquake.org

G. F. Panza
Beijing University of Civil Engineering and Architecture (BUCEA), Beijing, China

and Lithosphere Asthenosphere boundary depths of 37 and 63 km were observed in Eastern Anatolian Accretionary Complex. The thin mantle lid in this region has affected the whole crust in such a way that we observed the lowest shear velocities inside the crust in this region. We observed a significant thickening of both crust and lithosphere in Sanandaj–Sirjan Metamorphic zone comparing to Urmieh Dokhtar Magmatic Arc and Zagros Folding and Thrust Belt on its two sides.

1 Introduction

Considering the dispersion characteristics, surface wave analysis has the capability to provide us with significant information about the Earth's interior. Thanks to surface wave tomographic methods (e.g., Levshin et al. 1992; Ritzwoller et al. 2002), we can obtain the distribution of group velocities across any region and study their correlation with the known tectonic units and geological features (e.g., Levshin et al. 1992). In regions characterized by high seismicity and availability of a large number of seismic stations, like North-West (NW) Iran and its surroundings, the fulfillment of such studies could be particularly effective in investigations of crust and upper mantle structure.

In this study, NW Iran and surrounding areas is the region in the latitude range from 35° to 41° N and the longitude range from 42° to 50° E (Fig. 1). In this region, several tectonic processes are active that make it very interesting for seismological studies. This region has been the subject of several independent studies including surface wave tomography (e.g., Mangino and Priestley 1998), but two main problems are common to most of them: (1) the lateral resolution is worse than the dimension of the investigated tectonic units; (2) the studies did not cover the junction of NW Iran with surrounding areas. In this study, we improve the resolution and include NW Iran and surrounding areas with the aim to discuss about tectonic units and geological features as well. For this purpose, we use the data from local and regional earthquakes and obtain Rayleigh wave group velocity maps across NW Iran in the period range from 7 to 80 s, as described in the next sections.

NW Iran is surrounded by Eastern Anatolia in the West, the Lesser Caucasus (LC) and Kura Depression (KD) in the North, the Zagros Mountains and Central Iran (CI) in the South, and the South Caspian Basin (SCB), Talesh (TAL), and Alborz (ALB) Mountains in the East. The crust and upper mantle structure of this region is strongly affected by the Arabian–Eurasian collision. The convergence and assemblage of several continental pieces in the south of the Eurasian plate has led to the formation of this region (Sengor 1990).

Eastern Anatolia is divided into three tectonic segments (Fig. 1) named as Pontides (PT), Eastern Anatolian Accretionary Complex (EAAC), and Bitlis-Massif (BM) metamorphic zone in the north, middle, and south, respectively (e.g., Sengor et al. 2003). Pontides is a magmatic area resulting from a subduction, EAAC, which has no continental-origin basement, is mainly made by ophiolitic melange and flysch, and Bitlis-Massif metamorphic zone is the result of the collision of Menderes–Taurus block (western frame of EAAC) and Arabian plate (Sengor et al. 2003).

Widespread volcanism between the Eocene to Quaternary in NW Iran and eastern Anatolia is one of the main characteristics of the Arabian–Eurasian convergence (Agard et al. 2011; Yilmaz 1990; Keskin et al. 1998; Chiu et al. 2013). The distribution of volcanic rocks and major volcanoes are mapped in Fig. 1. Sahand (3707 m) and Sabalan (4811 m) are the two volcanoes in NW Iran that dominate the landscape of the region. In eastern Anatolia, there are several major volcanoes, starting from west and north of Lake Vane and extending to the north and northeast. Ararat (5137 m), Tendurek (3584 m), Girekol (2145 m), and Suphan (4158 m) are the most important volcanoes in eastern Anatolia and, somehow, they control the landscape of their adjacent regions (Fig. 1).

The SCB and the KD are a rigid block considered as the relics of a larger back arc basin related to the Tethyan subduction (e.g., Mangino and Priestley 1998; Brunet et al. 2003). The basement of SCB is a relatively thick (∼13 km) and high-velocity oceanic-like crust that is covered by extremely thick (∼20 km) and low shear wave velocity sediments (Mangino and Priestley 1998; Brunet et al. 2003; Knapp and Connor 2004). Although an under-thrusting beneath the Talesh and Alborz Mountains in the SCB is a highlighted characteristic of its current tectonics (Bavali et al. 2016; Jackson et al. 2002), relocation of local events indicates that it is not widespread (Zanjani et al. 2013).
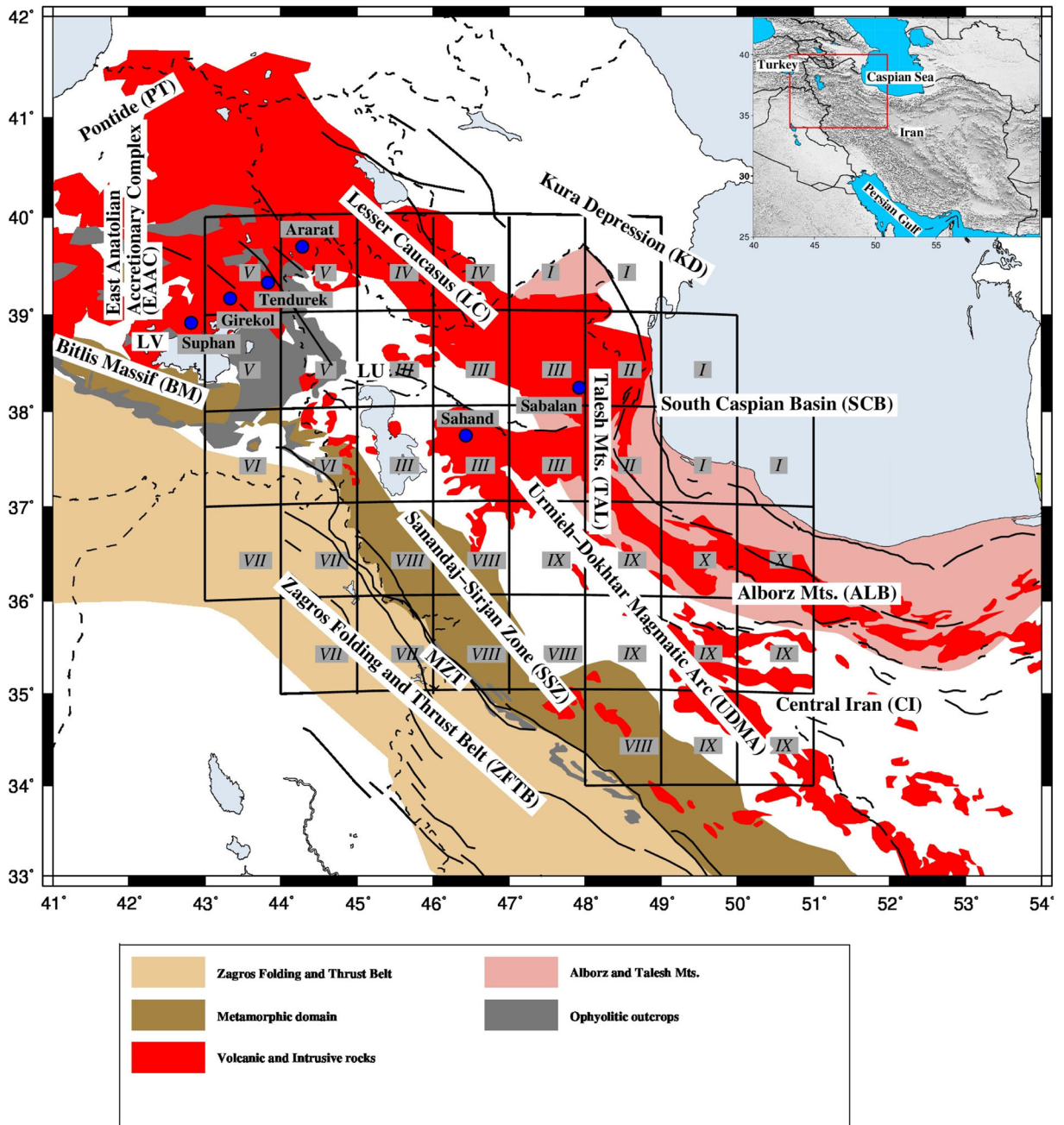
Fig. 1 Tectonic units of NW Iran and surrounding areas (from National Geoscience Database of Iran, http://www.ngdir.ir). Solid lines indicate the major active faults, modified from Hessami et al. (2003). Blue circles denote the prominent volcanoes in the region. The region is gridded for tomographic purposes (dispersion curve averaging) by 1° × 1° cells, identified with Latin numbers. A large-scale map of the region is plotted on the top right of the figure. MZT, Main Zagros Thrust; LU, Lake Urmieh; LV, Lake Van

Tectonically, Zagros mountain range consists of several segments with NW–SE elongation and parallel to each other. The Main Zagros Thrust fault (MZT in Fig. 1) is considered as the suture between the Arabian plate and Central Iran block, after the closure of Neotethys Ocean (e.g., Stocklin 1968; Talebian and Jackson 2002). Stocklin (1968) classified the Zagros range to three main tectonic units (Fig. 1). The region in the southwest of the MZT is called Zagros Folding and Thrust Belt (ZFTB). The significant characteristic
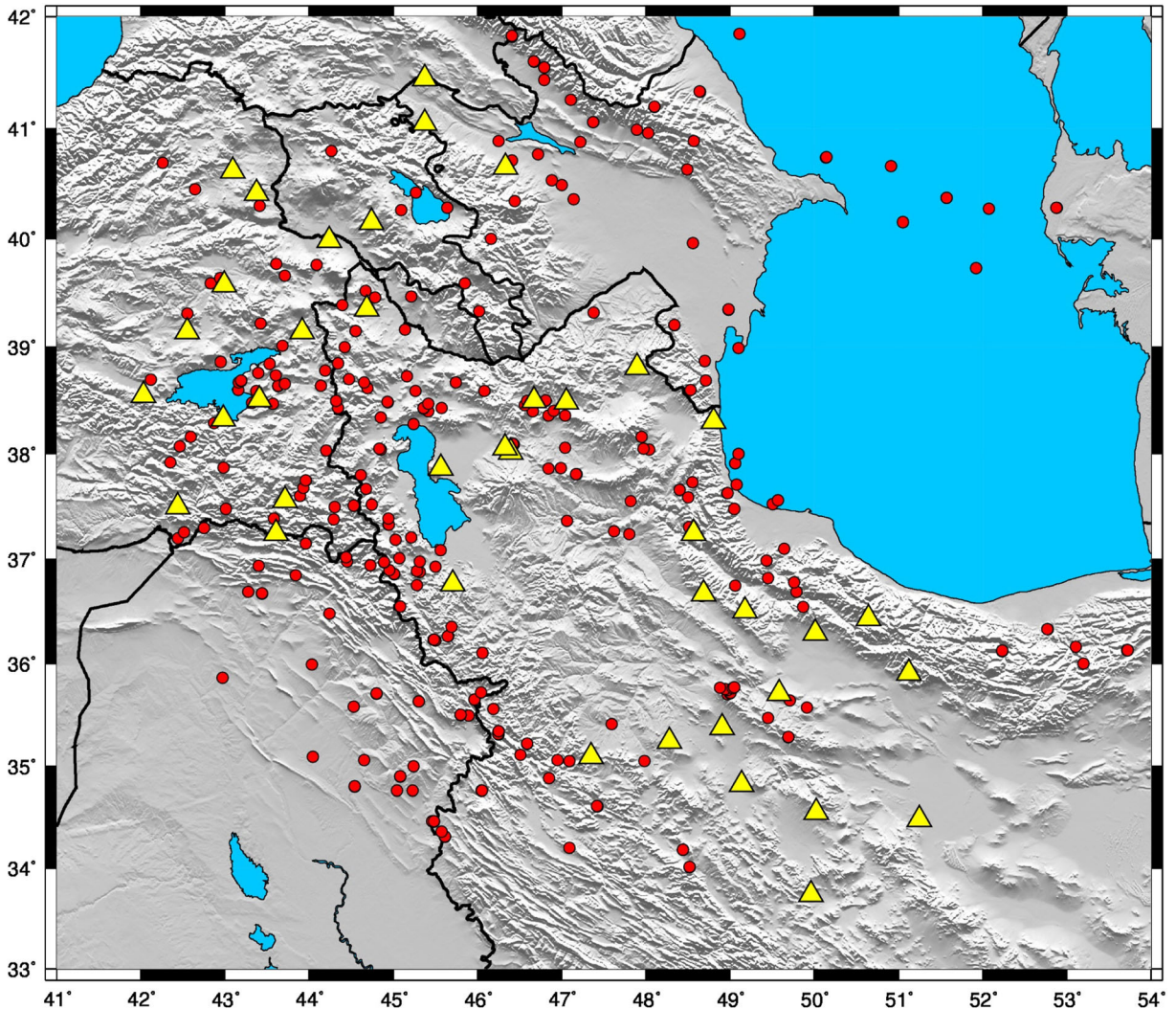
Fig. 2 Geographical distribution of the 39 seismic stations (yellow triangles) and of the epicenters (red circles) of the 280 earthquakes considered in this study, on shaded topography map

of this zone is the thick sequence of sediments (approx-imately 6–12 km) over an altered Precambrian basement (e.g., Giese et al. 1984; Stocklin 1968) and the presence of many hidden and active reverse faults resulting from surface folding (Jackson and Fitch 1981). Another tectonic segment is the Sanandaj–Sirjan Zone (SSZ), located in the northeast of MZT. SSZ is a metamorphic zone, with a width of 150–250 km, elongated parallel to the Zagros range. As can be seen from Fig. 1, the E–W-trending Bitlis-Massif metamorphic zone is the extension of SSZ into eastern Anatolia. The third tectonic segment of Zagros is the Urmieh–Dokhtar Magmatic Arc (UDMA) in the northeast of SSZ, formed by intrusive volcanic rocks. The volcanic activity of this zone is

related to the Neotethys subduction with peak time of activity in Eocene (Alavi 1994).

Using the distribution of earthquakes locations, Talebian and Jackson (2004) and Maggi et al. (2000) indicate that the present-day seismicity of the Zagros range is relatively high and limited to ZFTB, while the SSZ and UDMA are almost devoid of seismic activity. Majority of the seismic events have shallow focal depths, ranging from 8 to 14 km (Talebian and Jackson 2004). Jackson and Fitch (1981) thought that the reason for the wide distribution of earthquakes in ZFTB is the presence of hidden and active reverse faults resulting from the movement of old faults that are reactivated during the continental collision.

Table 1 Coordinates and network information of the stations considered in this study

Station code	Longitude (°)	Latitude (°)	Elevation (m)	Network code	Network name
FTBB	46.3944	38.0171	1665	IRSC	Iranian Seismological Center
TABZ	46.326599	38.056801	1487	IRSC	Iranian Seismological Center
TAHR	47.0513	38.489498	1413	IRSC	Iranian Seismological Center
TVRZ	46.6675	38.5042	1693	IRSC	Iranian Seismological Center
MAHB	45.705399	36.766602	1370	IRSC	Iranian Seismological Center
HKZM	48.904499	35.377499	2328	IRSC	Iranian Seismological Center
HSRG	48.278702	35.241798	2545	IRSC	Iranian Seismological Center
HAGD	49.139	34.822	1831	IRSC	Iranian Seismological Center
QABG	49.582401	35.7085	2085	IRSC	Iranian Seismological Center
QALM	50.6465	36.431999	2212	IRSC	Iranian Seismological Center
QCNT	50.009102	36.2901	1319	IRSC	Iranian Seismological Center
QSDN	49.174	36.503601	2148	IRSC	Iranian Seismological Center
ASAO	50.025002	34.548	2217	INSN	Iranian National Seismological Network
CHTH	51.125999	35.908001	2350	INSN	Iranian National Seismological Network
ZNJK	48.685001	36.669998	2200	INSN	Iranian National Seismological Network
GRMI	47.894001	38.810001	1300	INSN	Iranian National Seismological Network
MAKU	44.682999	39.355	1730	INSN	Iranian National Seismological Network
SNGE	47.347	35.092999	1940	INSN	Iranian National Seismological Network
GHVR	51.25	34.48	927	INSN	Iranian National Seismological Network
KHMZ	49.959	33.739	1985	INSN	Iranian National Seismological Network
CLDR	43.9172	39.144	2094	KO	Kandilli Observatory BB and SM Stations
VANB	43.4058	38.509	1227	KO	Kandilli Observatory BB and SM Stations
CUKT	43.6077	37.2473	1298	KO	Kandilli Observatory BB and SM Stations
TASB	44.2384	39.9839	849	KO	Kandilli Observatory BB and SM Stations
MLAZ	42.5496	39.141	1581	KO	Kandilli Observatory BB and SM Stations
AKDM	42.98	38.3285	1662	KO	Kandilli Observatory BB and SM Stations
AGRB	42.992	39.5755	1820	KO	Kandilli Observatory BB and SM Stations
SIRT	42.4392	37.501	1038	KO	Kandilli Observatory BB and SM Stations
GURO	42.0322	38.5509	1388	KO	Kandilli Observatory BB and SM Stations
KARS	43.0937	40.6152	1747	KO	Kandilli Observatory BB and SM Stations
DIGO	43.3742	40.4147	2278	TU	National Seismic Network of Turkey
HAKT	43.71	37.56	2153	TU	National Seismic Network of Turkey
DGRG	45.37317	41.45072	690	GO	National Seismic Network of Georgia
GNI	44.74	40.15	1609	IU	IRIS/USGS
GANJ	46.3297	40.6519	560	AB	National Seismic Network of Azerbaijan
QZX	45.372	41.048	574	AB	National Seismic Network of Azerbaijan
SARA	45.5654	37.8634	1318	IASBS	Institute for Advanced Studies in Basic Sciences
KUTE	48.8038	38.3046	116	IASBS	Institute for Advanced Studies in Basic Sciences
BRND	48.568	37.2483	549	IASBS	Institute for Advanced Studies in Basic Sciences

Crustal thickness in NW Iran and surrounding areas has been investigated in several independent studies (Asudeh 1982; Dehghani and Makris 1984; Mangino and Priestley 1998), implying that the average crustal thickness beneath the NW Iran is approximately in the range from 40 to 50 km. Based on receiver function studies, Taghizadeh-Farahmand et al. (2010) and Zor et al. (2003) found an average Moho depth of about 48 and 45 km in NW Iran and eastern
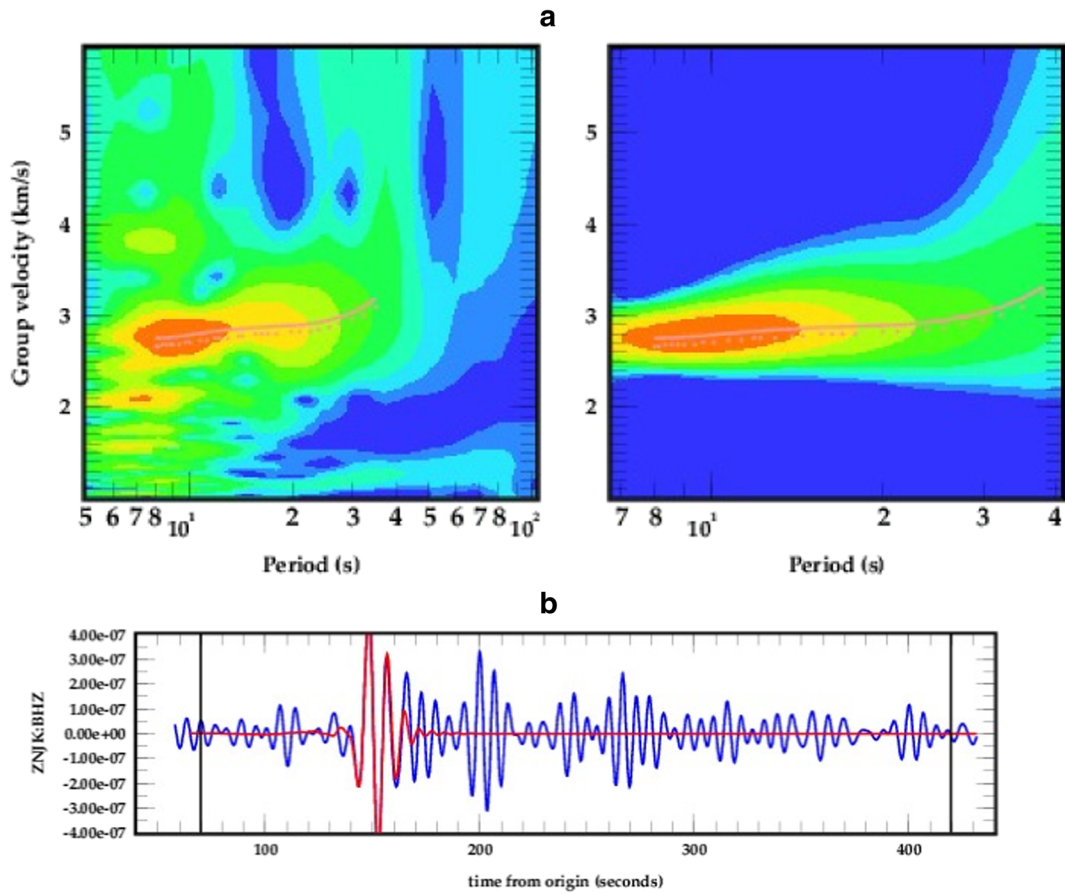
Fig. 3 Example of dispersion curve extraction by FTAN from the vertical component of an event recorded by ZNJK station that occurred at 13:22:23 UTC on 25 June 2013, with Ml = 4.1 epicenter coordinates (44.65° N, 38.67° E) and focal depth of 7.3 km. **a** The FTAN diagram of raw filtered waveform and calculated fundamental mode are mapped at left and right, respectively. The selected dispersion curve is shown by dotted line. **b** The filtered raw waveform (blue line) and its extracted fundamental mode (red line)

Anatolia, respectively. More recently, Mortezanejad et al. (2013) calculated a Moho depth of about 48 km in the southeast of Sabalan volcano and increasing to ∼ 58 km beneath the Talesh Mountains. In Zagros, based on receiver function studies along two seismic profiles crossing the Zagros belt, a sudden thickening beneath the SSZ has been observed by Paul et al. (2006, 2010).

Many studies have been performed to investigate the mantle structure of NW Iran and surrounding areas: for example, using Pn tomographic method, Al-Lazki et al. (2003; 2004; 2014) pointed a partially molten to absent mantle lid beneath the NW Iran and surrounding areas. Other studies (e.g., Sengor et al. 2003; Keskin 2003; Maggi and Priestley 2005) found a rather similar result implying that the lithospheric mantle in NW Iran and eastern Anatolia is thinned or absent. Al-Lazki et al. (2003) observed high Pn velocities beneath the northern Arabian plate implying that it possesses a stable

lithospheric mantle. Taghizadeh-Farahmand et al. (2010) in NW Iran and Gok et al. (2007) in eastern Anatolia obtained an average LAB (lithosphere–as-

Table 2 Number of paths and average distance for each considered period

Period (s)	Number of paths	Average distance (km)
7	857	348
10	1079	378
20	1042	409
35	749	442
40	650	449
55	320	454
60	267	459
70	152	463
80	55	500
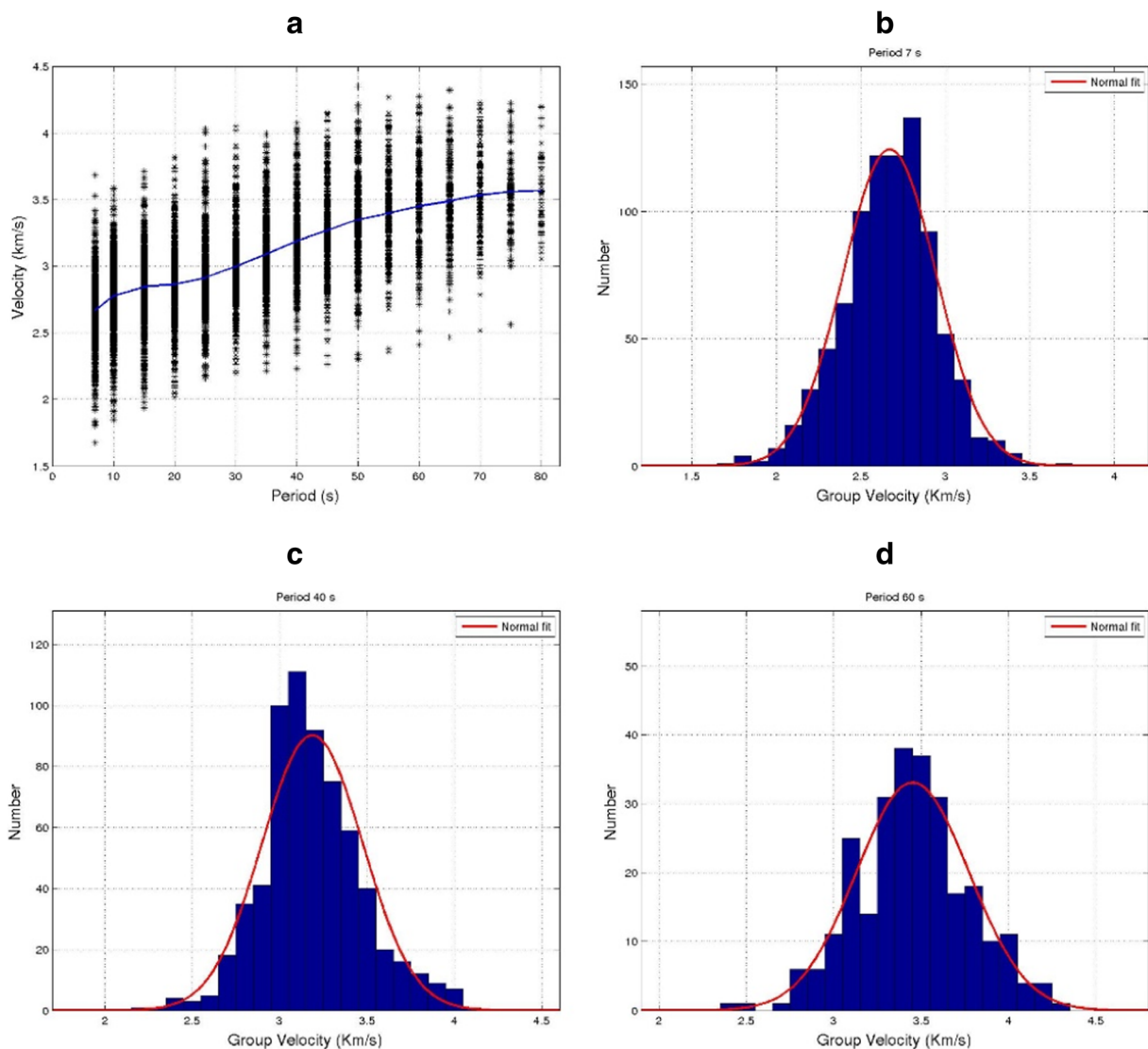
Fig. 4 **a** Distribution of input data (black stars) and its average (blue line) for the period range 7–80 s. **b**–**d** Histogram distribution and normal fit of probability density function of observed data for periods 7, 40, and 60 s, respectively

thenosphere boundary) depth of about 85 and 70 km, respectively. Their result is consistent with the result of Priestley et al. (2012) that, based on surface wave tomography, observed a thin mantle lid in NW Iran and eastern Anatolia that is trapped by a thicker one in the South Caspian and Zagros. Their result is the most important conclusion of all the aforementioned studies.

2 Data

To build the database for the surface wave analysis, we selected 280 earthquakes that occurred within NW Iran and surrounding areas between 2005 and 2015, with focal depths < 30 km and magnitudes > 3.0, from the catalog of the Iranian Seismological Center (IRSC). Waveform records from medium- and broad-band instruments belonging to national and international seismic networks have been used (Fig. 2). The Iranian national stations set contains 3 temporary stations from the Institute for Advanced Studies in Basic Sciences (IASBS), 8 permanent stations from the Iranian National Seismological Network (INSN), and 12 permanent stations from the IRSC of the Institute of Geophysics of University of Tehran (IGUT); the international stations set contains 2 stations from the National Seismic

Fig. 5 a V_s model, obtained by inverting the average observed dispersion curve (blue line from Fig. 4a) of the region. **b** V_s sensitivity kernels of the fundamental mode of Rayleigh waves computed, at periods ranging from 7 to 60 s, from the model shown in (**a**)
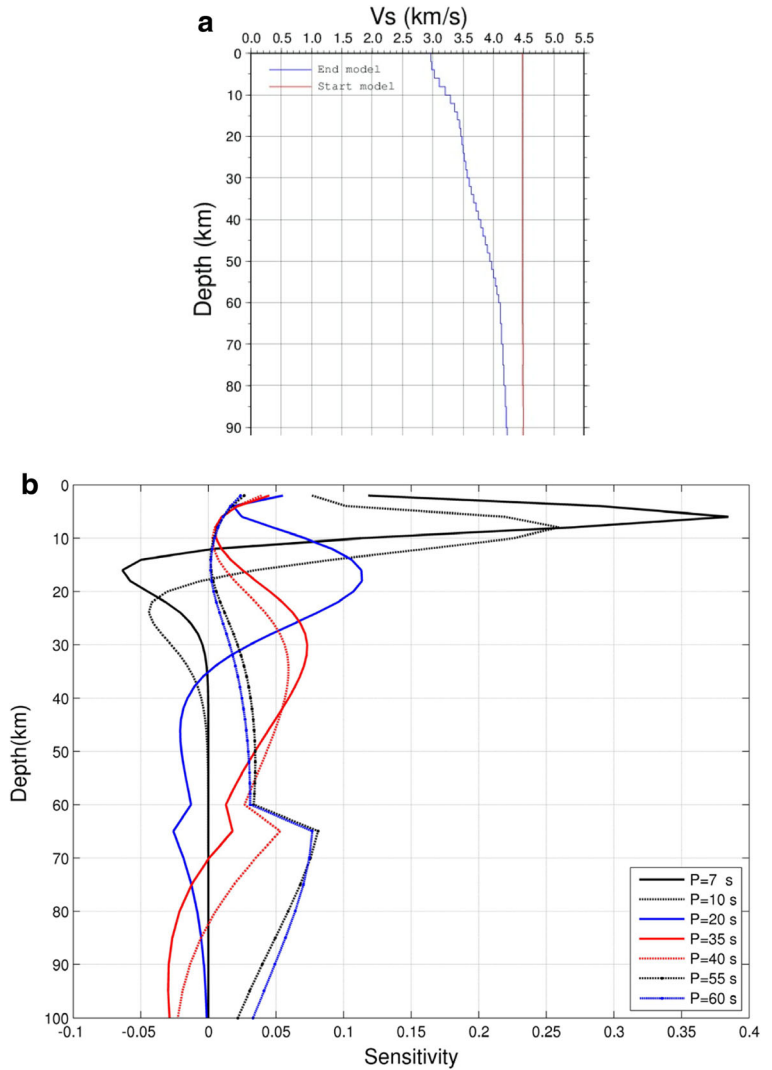
Network of Turkey (TU), 2 stations from the National Seismic Network of Azerbaijan (AB), 10 stations from the Kandilli Observatory Broad Band and Strong Motion Stations (KO), 1 station from the National Seismic Network of Georgia (GO), and 1 station from the IRIS/USGS (IU). The seismic records of the international stations set can be downloaded from the European Integrated Data Archive (EIDA); the codes, coordinates, and operation network of the mentioned stations are given in Table 1. The distribution of stations is non-uniform in the region: it is sparse in North, North-East, and South-West of the study area while in the rest, it is dense. The initial number of considered events was 1734 with a non-uniform distribution, localized along main active faults in the region. In order to reduce the

effect of such non-uniformity on the distribution of events-station paths, we used a program to scan the region by a window of 0.5 by 0.5 degrees and selected the first two events with the largest magnitude and signal-to-noise ratio, and that have been recorded by the majority of the stations. The distribution of the selected events is shown in Fig. 2, with the range of the event–station distances varying from 50 to 1050 km.

3 Methodology: dispersion measurements, tomography, and inversion

The first step for the calculation of surface waves dispersion curves is the exploratory analysis of the
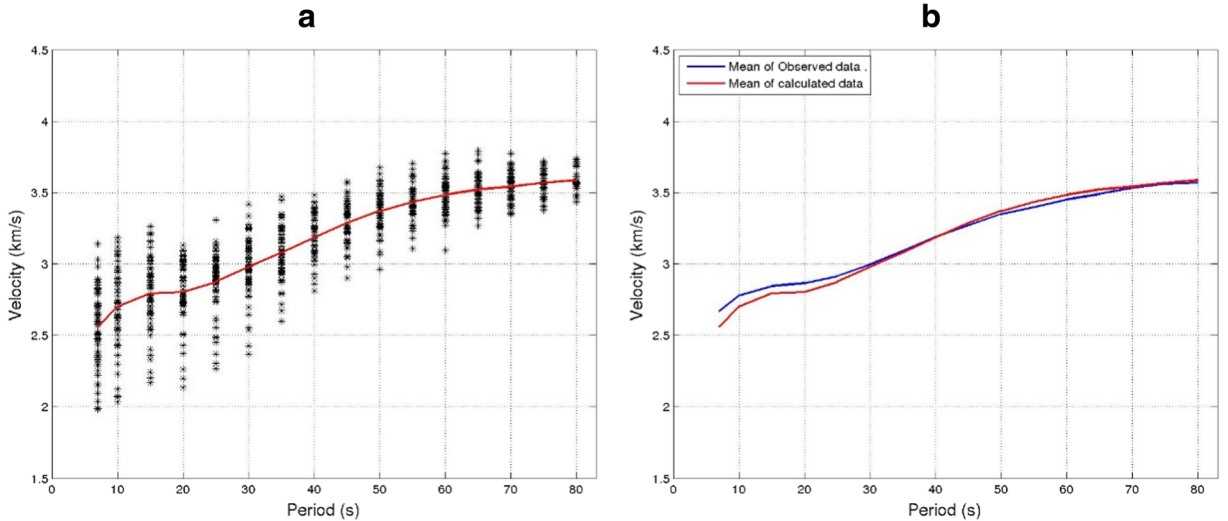
Fig. 6 a Distribution of output data (black stars) at grid nodes with a resolution length less than 150 km and its average (red line) for the period range 7–80 s. **b** Average of input data (blue line, from Fig. 4a) and output data (red line from panel **a**)

waveform data to select the events with acceptable signal-to-noise ratios; then, the Rayleigh dispersion curves have been extracted from the vertical component of the velocity records, after removing the instrument responses given by the calibration sheet of the instruments. The time domain signals have been decimated to five samples per second and, then, the baseline was obtained by removing the mean and trend. We used the frequency–time analysis (FTAN) method (Levshin et al. 1972, 1992) to estimate surface wave group velocities. Figure 3 shows an example of FTAN analysis performed on a selected event from our database for the dispersion curve extraction.

The process has been applied to each event–station path: the number of observed and accepted Rayleigh wave group velocities and the average of path length, ranging from 350 to 500 km, for each period, in the range from 7 to 80 s, are shown in Table 2. The event-station paths coordinates and group velocities for periods of 7, 10, 20, 35, 40, 55, and 60 s are shown in Tables S1–S7 in the electronic supplement. The distribution of all observed dispersion curves, with their mean, is shown in Fig. 4a. In Fig. 4b–d, we present the histogram distribution and normal fit of probability density function (PDF) of observed data for periods of 7, 40, and 60 s.

We used the inversion technique developed by Ditmar and Yanovskaya (1987) to produce the local group velocity maps at selected periods. The result of this tomography technique is the distribution of group velocities at different grid points throughout the region, which are used to produce group velocity maps. For each period, the tomographic method finds the solutions of group velocities, $V(x, y)$, that minimize the following function:

$$(d-Gm)^T(d-Gm) + \alpha \iint |\nabla m(x,y)|^2 dxdy = min$$

in which $d = t-t_0$ is input data vector, t and t_0 are observed and computed travel time along each path, G is data kernel, and $m(x, y)$ is defined as:

$$m(x,y) = \left(V^{-1}(x,y)-V_0^{-1}\right)V_0$$

where x and y indicate, respectively, the longitude and latitude, $V(x, y)$ is the group velocity at point (x, y), V_0 is the reference average group velocity, and α is a parameter that controls the trade-off of smoothness and fitness of the output velocities. Increasing α parameter means increasing the smoothness and reducing the fitness and conversely.

To parameterize the resolution of solutions, Yanovskaya (1997) and Yanovskaya et al. (1998) introduced the concept of "averaging area" that is defined by an ellipse centered at point (x, y) with the largest and smallest axes a and b, respectively. The resolution in each point is the mean size of the averaging area, and is defined as $L = (a + b)/2$. Small and large values of L mean higher and lower resolution, respectively. They also introduced the parameter named "stretching" of the averaging area defined as $\varepsilon = 2(a - b)/(a + b)$ to evaluate the ray space

9

a

c

b

d
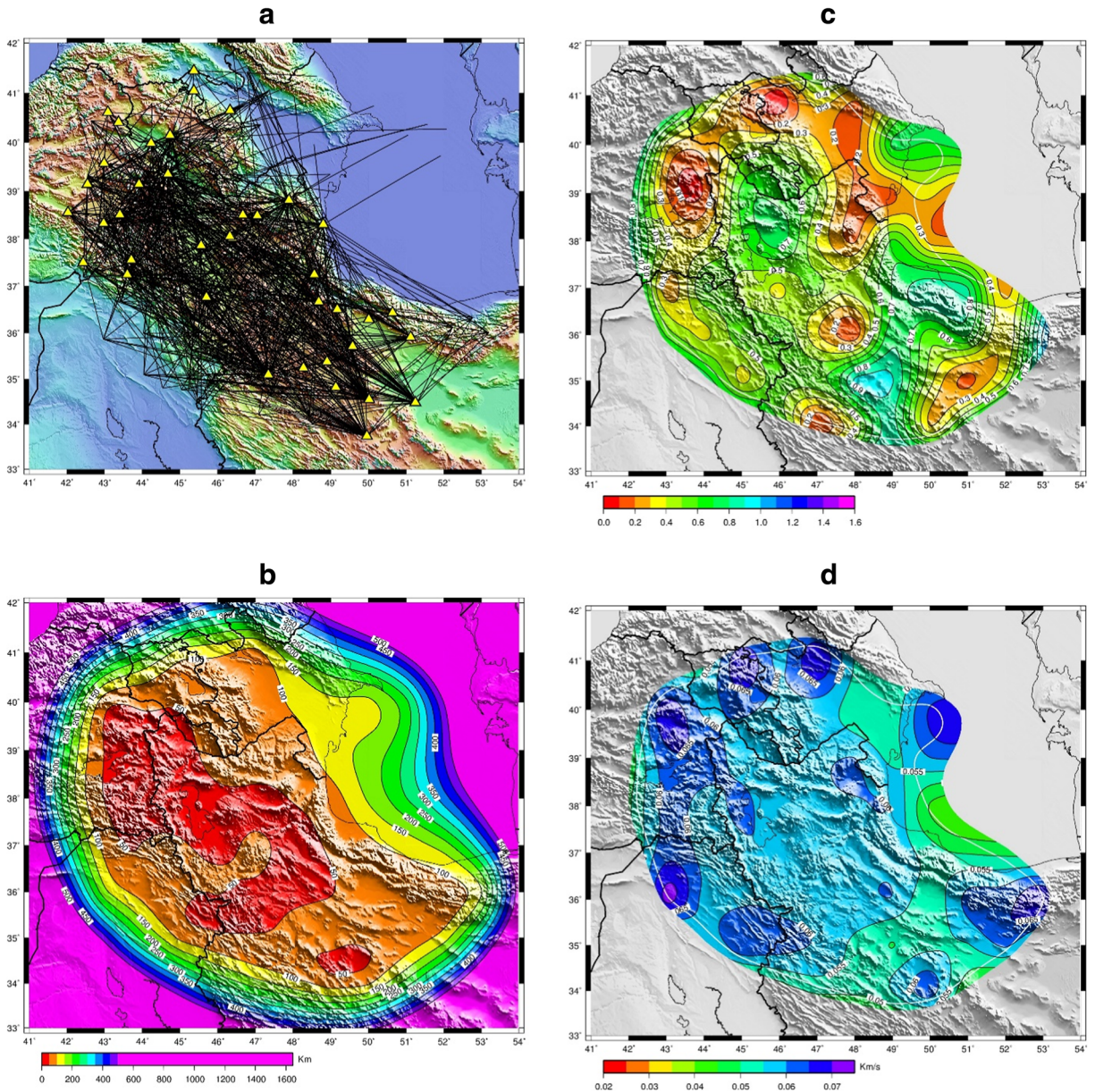
Fig. 7 Quantities controlling the quality of the tomographic maps for periods 7, 20, 40, and 60 s. **a** Path coverage (solid black lines) and stations (yellow triangles). **b** Averaging area. **c** Stretching parameter. **d** Estimated errors. In panel (**c**) and (**d**), the images are clipped by averaging area contour line of 200 km while the 150-km contour line of the averaging area is shown by solid white line

coverage heterogeneity ($0 < \varepsilon < 2$). If a equals b, the ellipse turns to a circle and ε equals zero implying that the path space coverage is uniform. If a is much larger than , the ellipse is like a line and ε equals to 2, implying that all the paths have a very clear preferred orientation.

Beside the group velocities, the distribution of corresponding standard errors, averaging area, and stretching parameter at different grid points of the study area is the final result of the tomographic procedure used. The root mean square (RMS) of travel times that are considered

20 s

a

c

b

d
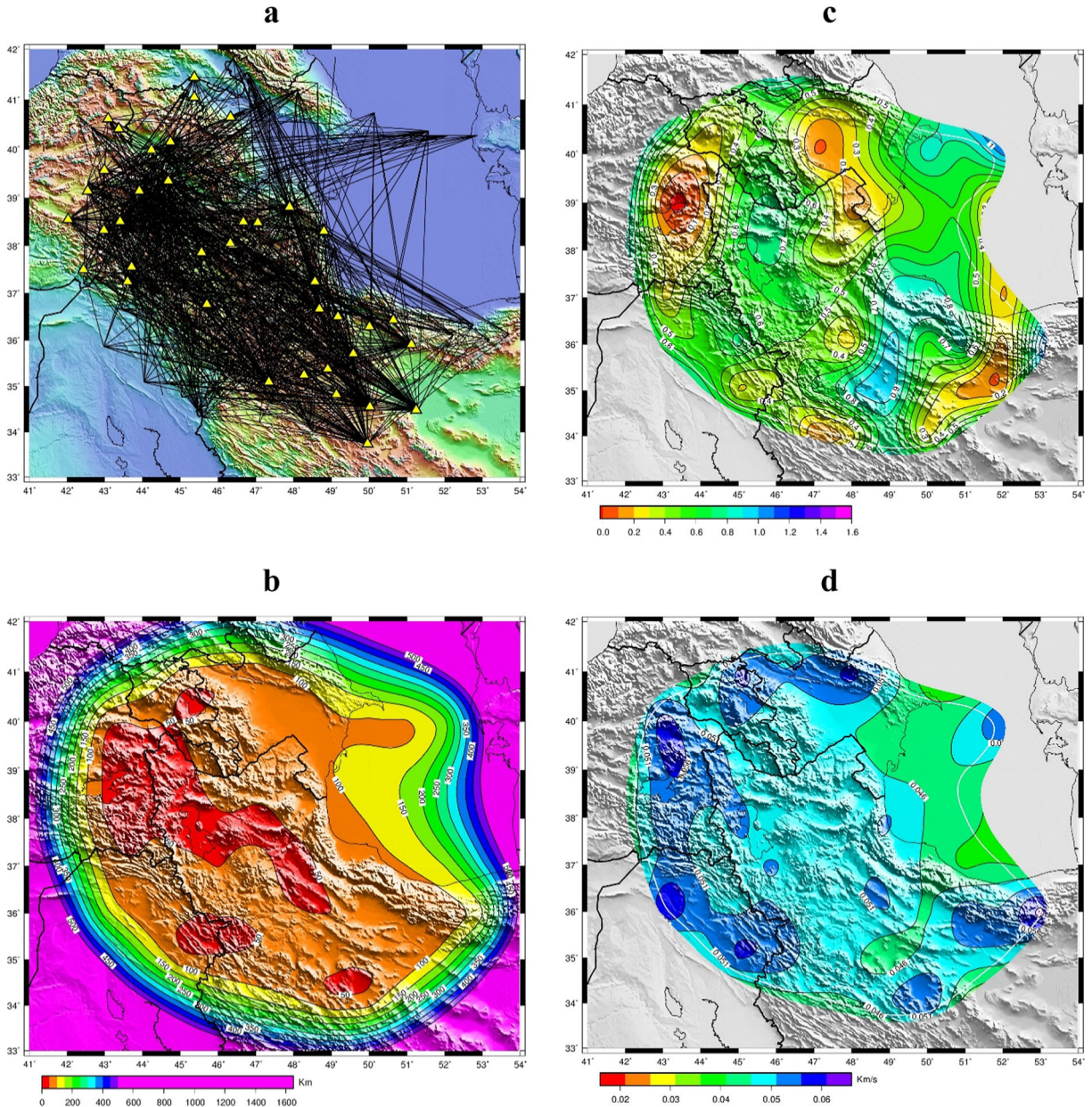
Fig. 7 (continued)

as standard errors of input data allow us to calculate the standard errors of the solutions.

In order to find quantitative information about the depth structure of the crust and upper mantle in the region, obtaining the shear velocity models from computed dispersion curves is essential. To compute the shear velocity model for a given dispersion curve, we used a non-linear inversion method known as "Hedgehog" (e.g., Panza

1981). This method that is well described by Karagianni et al. (2002) and Raykova and Panza (2010) is a Monte Carlo trial-and-error search on several parameters. Shear velocity (V_s), compressional to shear velocity ratio (V_p/V_s), thickness, and density are the layer parameters that can be fixed or variable during the inversion procedure. For each parameter, a range of variation is specified by a start value, step, and an upper and lower bound. The range of allowed

a

c

b

d
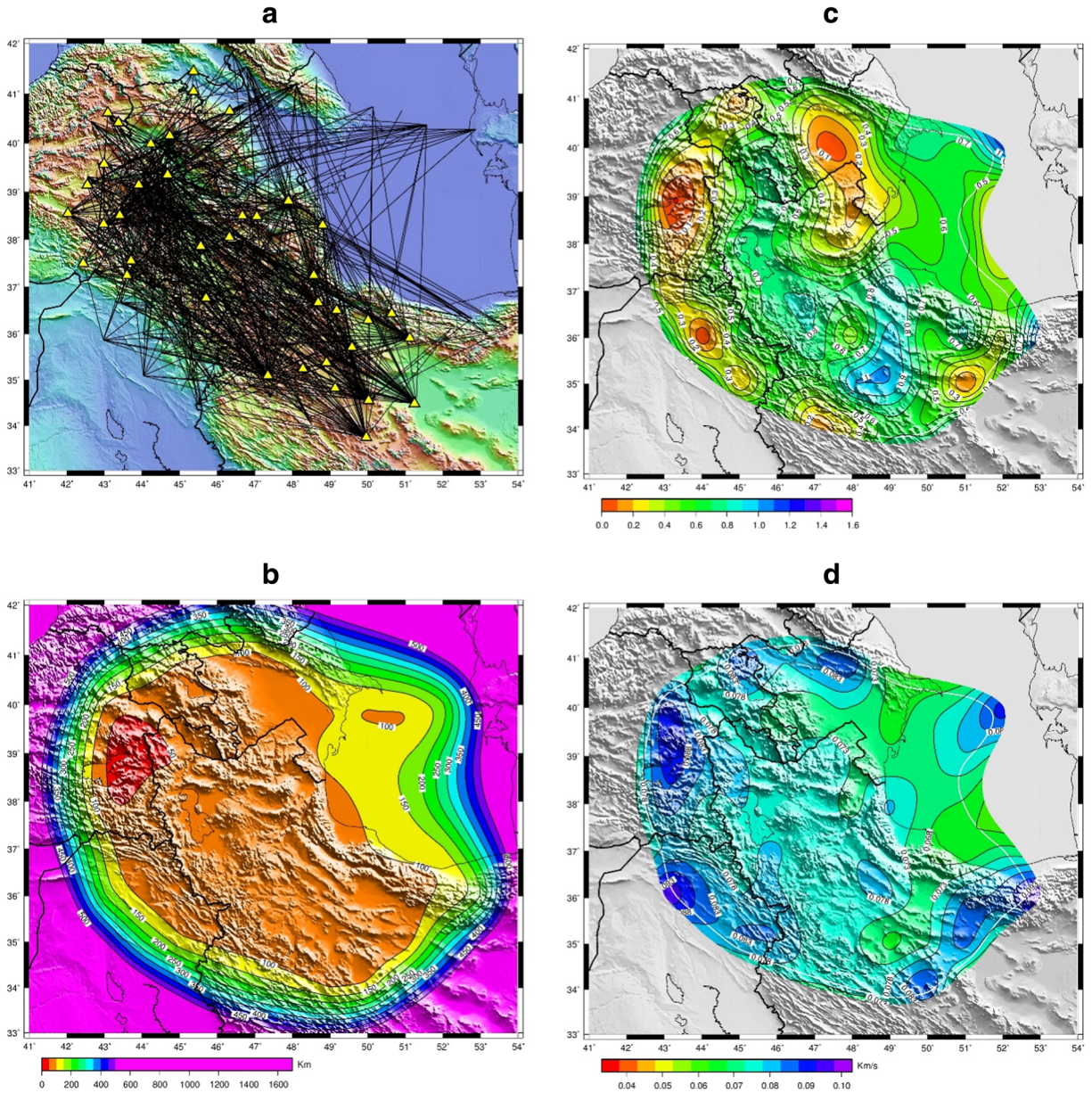
Fig. 7 (continued)

values for Moho depth and V_s within the crust and upper mantle is controlled by the available independent data from literature. A limited number of layers should be defined for the velocity model. Depending on the lowest period of the observed dispersion curves, the velocity and thickness of uppermost crustal structure must be fixed using the data from literature. The maximum depth of model is controlled by the longest period of the observed dispersion curve. To find the solutions, the method will try on many start

models. If the computed dispersion curve of each model at all periods fall within the corresponding errors and if the RMS of the theoretical and observed dispersion curve is less than a predefined value, the model is considered acceptable.

To obtain the shear velocity models from calculated dispersion curves, we gridded the study area to 1° by 1° cells. In order to do depth inversion, we selected the cells that are mostly located inside the averaging area contour
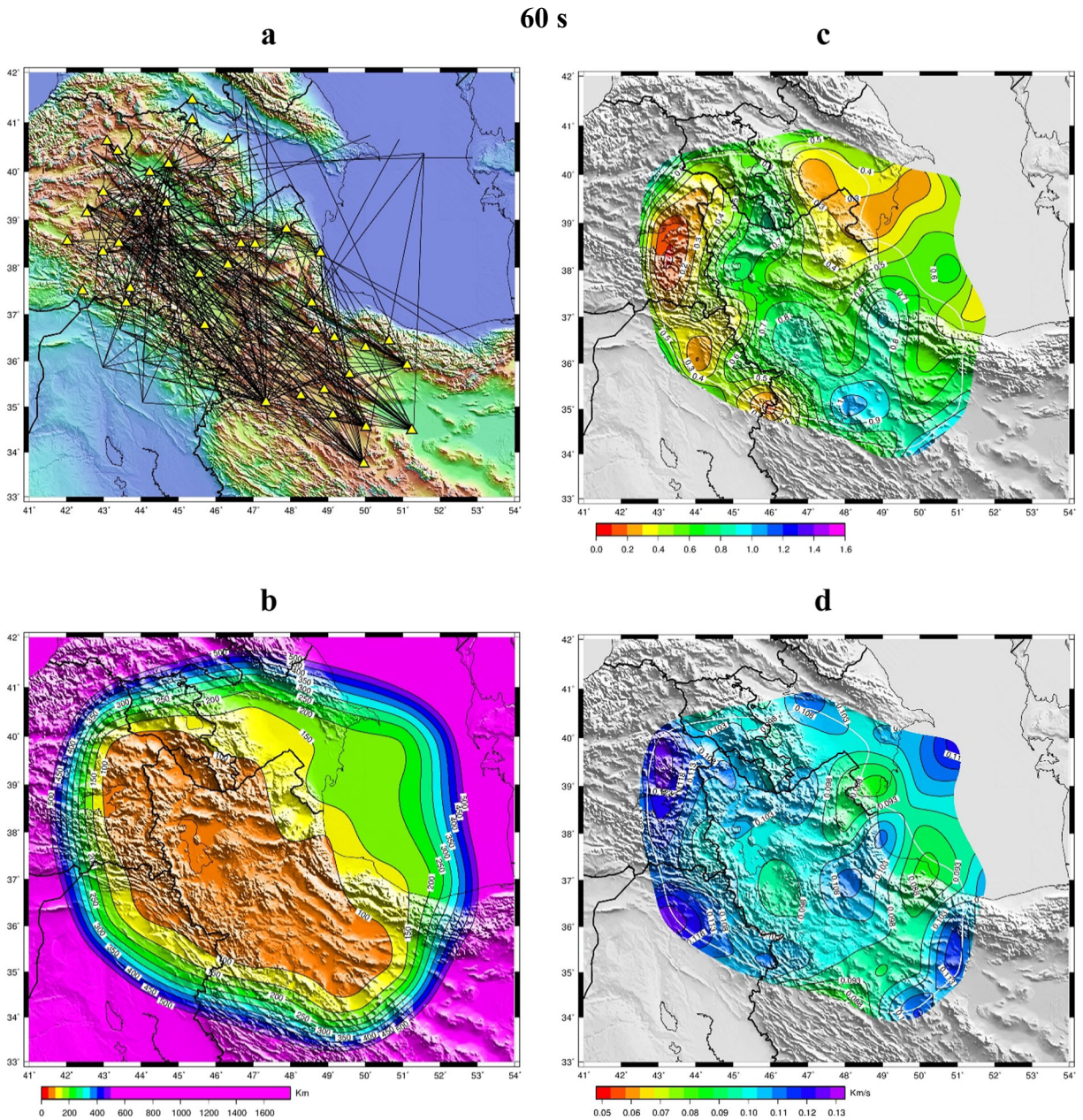
Fig. 7 (continued)

line of 150 km for the 60-s period. We calculated the dispersion curves of each cell by averaging the group velocities at four corners of the cell, for periods, T, from 7 to 60 s. We did not consider periods longer than 60 s in the inversion procedure because of the low ray coverage for $T > 60$ s. The error of group velocity at each period in a given cell is estimated as the average of the computed errors and standard deviation of group velocities at four

corner of the cell. To find the cells covering each tectonic unit, we plotted the selected cells on the map of Fig. 1 and marked the cells that mostly cover the same tectonic unit by the same Latin numbers from I to X. We calculated the mean dispersion curve of each tectonic unit by averaging the dispersion curves of all cells with the same labels (Fig. 1). Considering the same logic used in calculating errors in a typical cell, for each tectonic unit, the
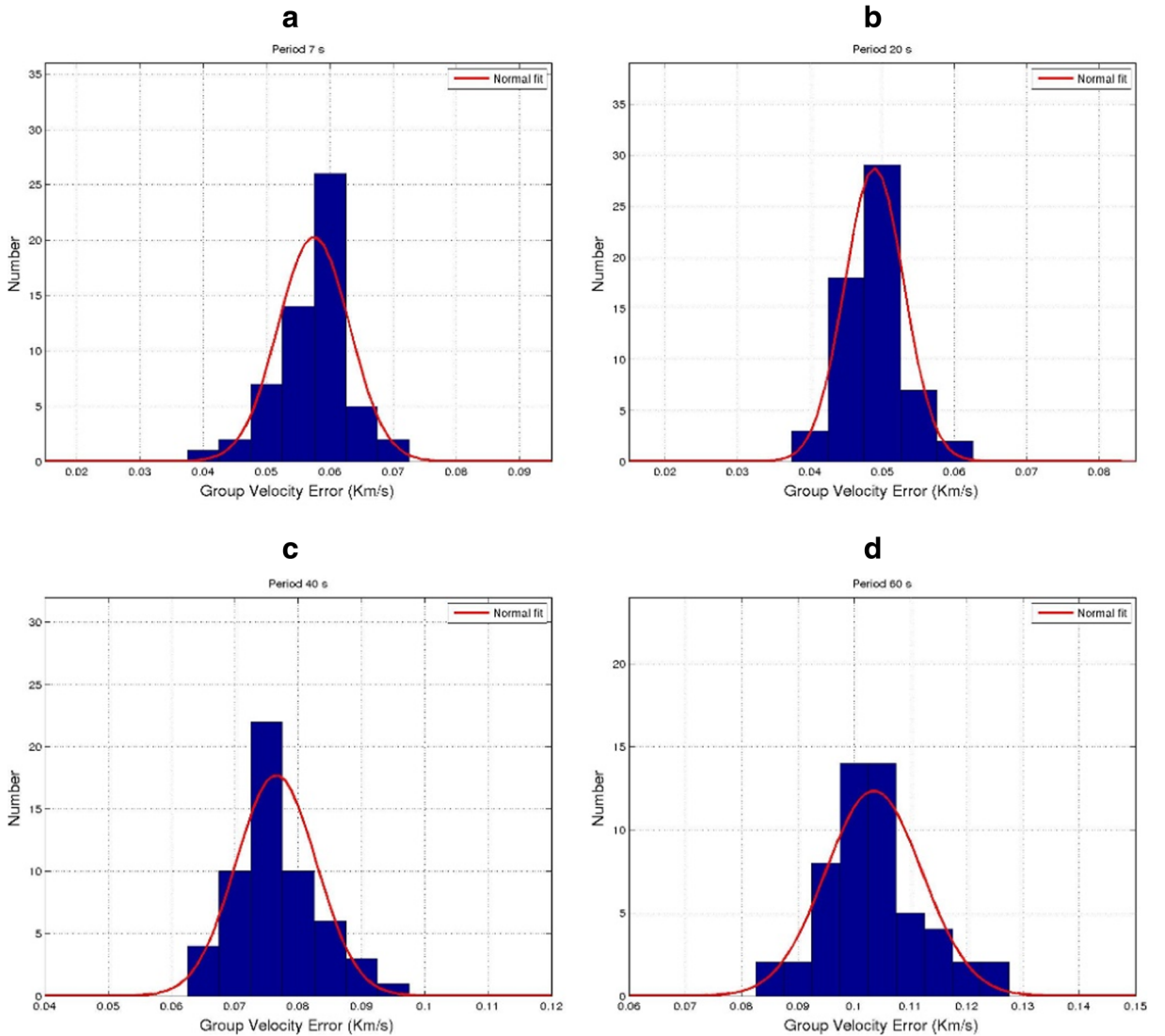
Fig. 8 a–d Histogram of distribution and normal fit of probability density function of velocity errors for periods 7, 20, 40, and 60 s, respectively

relevant errors of each period is estimated as the average of the errors and standard deviation of group velocities of all cells used in averaging.

To perform V_s versus depth inversion, we considered a five-layer velocity model, with variable V_s and thicknesses and fixed V_p/V_s and density for each layer. Taking into account the literature information about the crust and upper mantle, the variation range of V_s and thickness in all tectonic units is selected in a way that the three upper layers cover the crust and the remaining two cover the upper mantle. As the lowest period of our input dispersion curves is 7 s, we fixed the velocity of uppermost 3 km of the crust

using the values around group velocity of 7 s. As a rule of thumb, the maximum penetrating depth of surface waves is defined by $\frac{2}{3}\lambda$ where λ is wavelength. From Fig. 4d the range of group velocity for a period of 60 s is between 3.0 and 4 km/s, so the maximum depth will be in the range of 120 to 160 km. With this logic, we modeled the structures down to a maximum depth of 160 km. Below the five parameterized layers, we use a layer with fixed V_s equal to 4.5 km/s from ak135 global velocity model and a variable thickness for reaching the maximum allowable depth of 160 km. The ak135 global model is used for the rest of mantle.

14

a 7 s
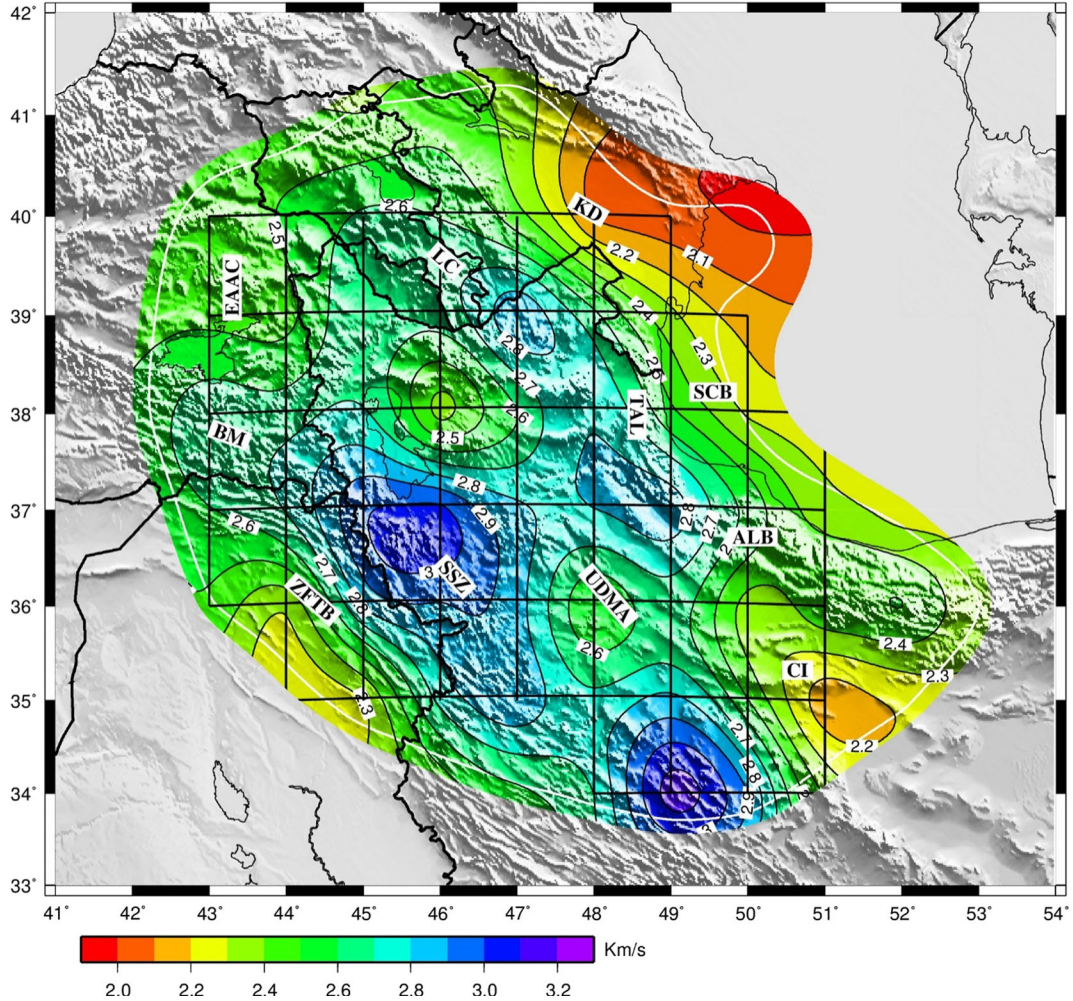
Fig. 9 a–d Tomographic image of the Rayleigh wave group velocities, for 7, 20, 40, and 60 s, respectively, on shaded topography map with main geographic and tectonic landmarks. The image is clipped by averaging area contour line of 200 km while the 150 km contour line of averaging area is shown by solid white line. The tomographic cells are plotted using solid black lines

4 Results

Rayleigh wave group velocity maps from 7 to 80 s have been produced. Three smoothing parameters, $\alpha = 0.1$, 0.2, and 0.3, have been used to calculate the group velocity maps and finally we selected the value of $\alpha = 0.3$ that leads to relatively smooth maps with small group velocity errors.

The estimation of the depth range influences the group velocities at each period can be done by computing the sensitivity kernels of Rayleigh waves (Panza 1981), using any pertinent structural model for the region. For the sake of simplicity, in order to obtain a suitable shear velocity model of the region, shown in Fig. 5a, the mean dispersion curve of the input data has been linearly inverted using Computer Programs in Seismology version 3.30 (Herrmann and Ammon 2004). With the inverted model, for the set of selected periods, i.e., 7, 10, 20, 35, 40, 55, and 60 s, the sensitivity kernels of Rayleigh waves have been computed (Urban et al. 1993) and are shown in Fig. 5b. The sensitivity kernels are then considered in the discussion, focusing on the relations between lateral variations of group velocities and known geological features, like sedimentary basins, crust, and upper mantle structures.

b 20 s
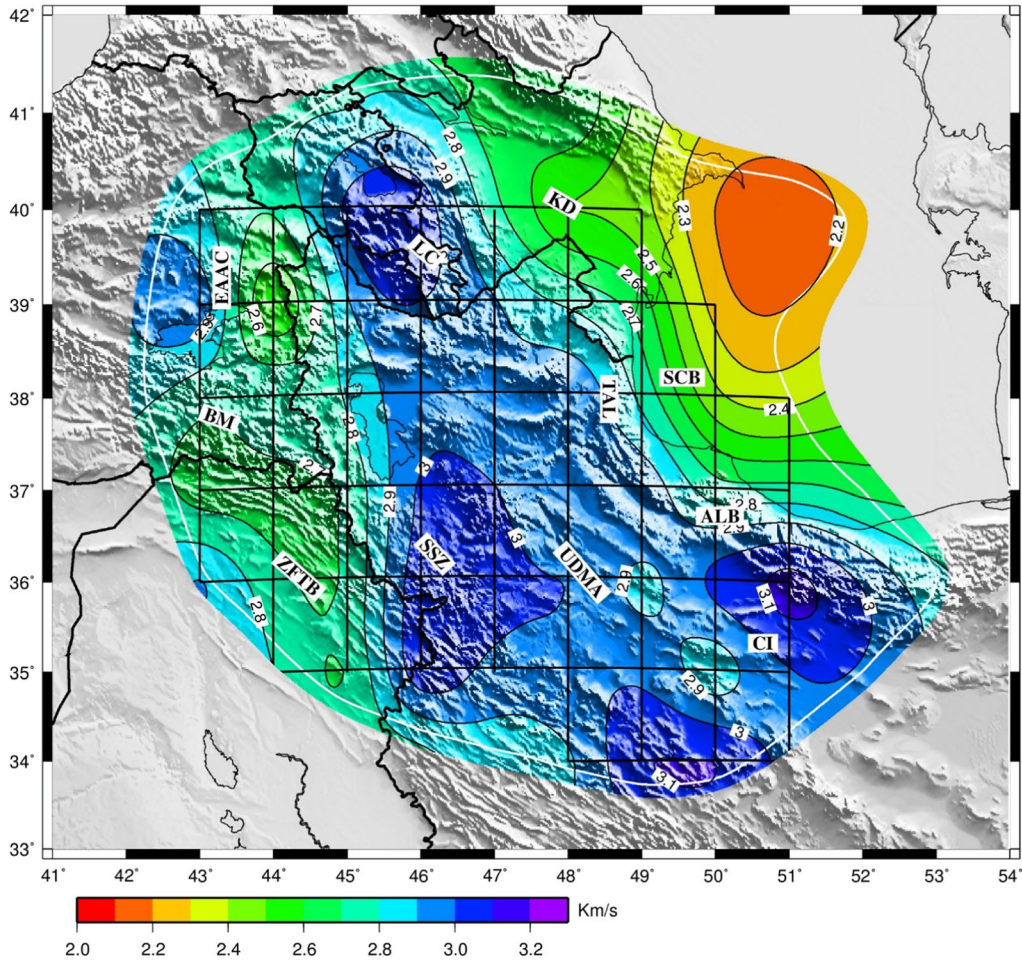
Fig. 9 (continued)

From the sensitivity kernels, it is clear that the shallow structures control the dispersion at short periods while longer periods are more influenced by deeper structures. Rayleigh waves at 7 s and 10 s are sensitive to the upper crust within a thickness less than 10 km. At 20 s, they sample the whole crust with the maximum sensitivity at about 20 km. Waves with 35-s and 40-s periods are mainly controlled by the lower crust and upper mantle, whereas the periods longer than 55 s are more sensitive to the uppermost mantle than to the lower crust mechanical properties.

To assess our results, we performed a test and compared the distribution and mean of all input data with output data in nodes with resolution length less than 150 km. The results of this test show small differences

between the mean of input and output data (Fig. 6a, b) and give a measure of the reliability of our results.

The quality controlling factors of the tomographic maps are shown in Fig. 7a–d for periods of 7, 20, 40, and 60 s. The event–station azimuthal path coverage of the study area is shown in Fig. 7a. Although the ray density decreases with increasing period, a "reasonably uniform" distribution of the ray paths is observed in the region for all periods. Inside the central part of the region where the path density and crossing is high, the "mean size of the averaging area," which can be considered as "resolution length," is less than 150 km while it increases rapidly in the rest of the region. We mapped the resolution length in Fig. 7b for the selected periods. Such maps provide us the size of resolvable velocity anomalies in the region. Inside the resolution contour

c 40 s
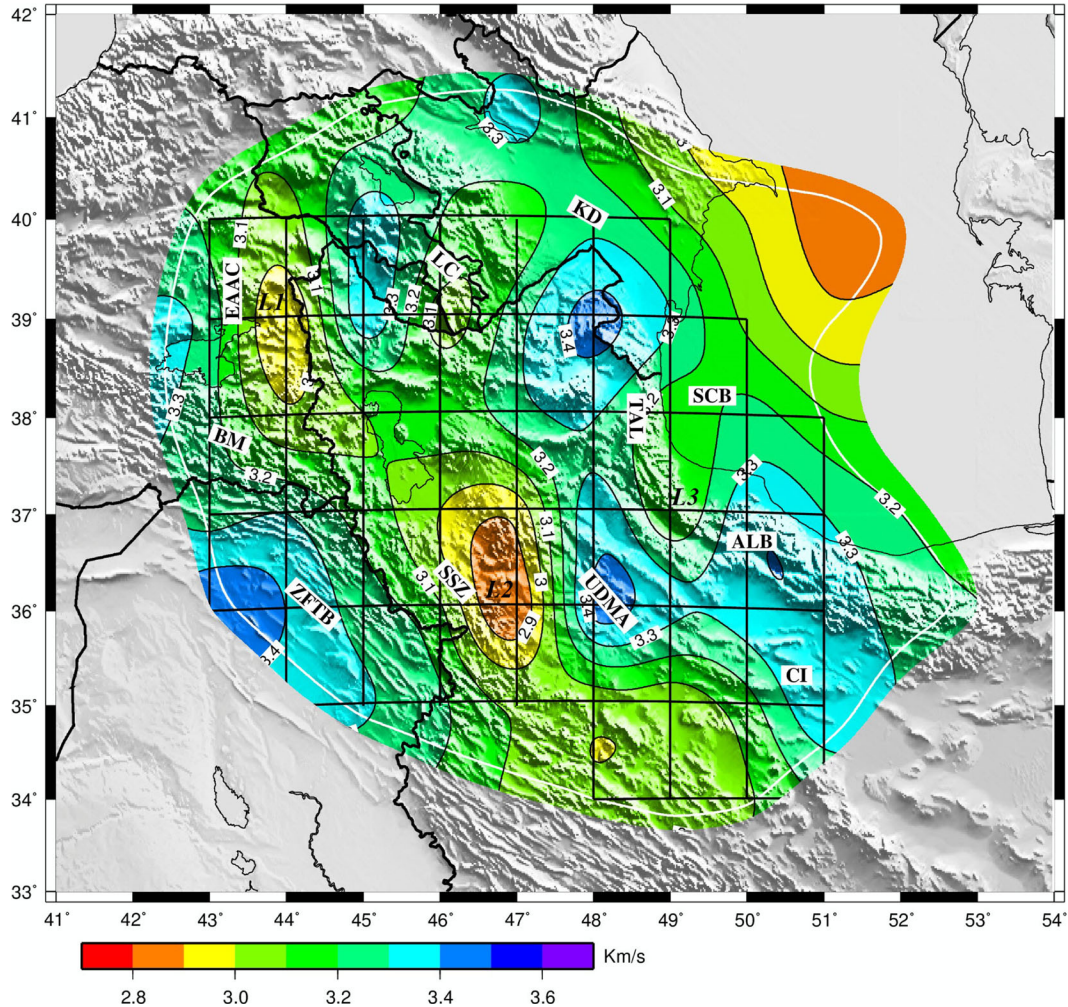
Fig. 9 (continued)

line of 150 km and in the central part of the maps, the predefined "stretching" parameter (Fig. 7c) is less than 1.0 and indicates relatively uniform path distribution in the region. This rather indicates that there is no smearing effect in the recovered Rayleigh group velocities. The corresponding errors of group velocities, varying from ~ 0.04 to ~ 0.12 km/s, are shown in Fig. 7d and reasonably increase with increasing period. Beside the spatial distribution of errors, its histogram distribution for each period gives an estimation of how well our tomographic maps computed the histogram of error distributions and normal fit of the probability density function, for the selected periods of 7, 20, 40 and 60 s, are plotted in Fig. 8a–d. In Fig. 9a–d, we map the group velocities only for the central part of the region where the resolution length is less than 200 km for all the considered periods.

The results of depth inversion of average Rayleigh dispersion curves for all the main tectonic units in the region are shown in Fig. 10a–j, where all the admitted solutions and corresponding calculated dispersion curves are presented by solid and dashed red lines, respectively. For any given tectonic zone, we have presented two velocity models; one is the minimum RMS solution and the other is the average of all the possible solutions. Both are plotted in Fig. 10a–j with black and blue lines, respectively. In Tables 3 and 4, the minimum RMS and mean velocity models for each tectonic zone are presented, respectively. Each velocity model is presented by six parameters: V1 to

d 60 s
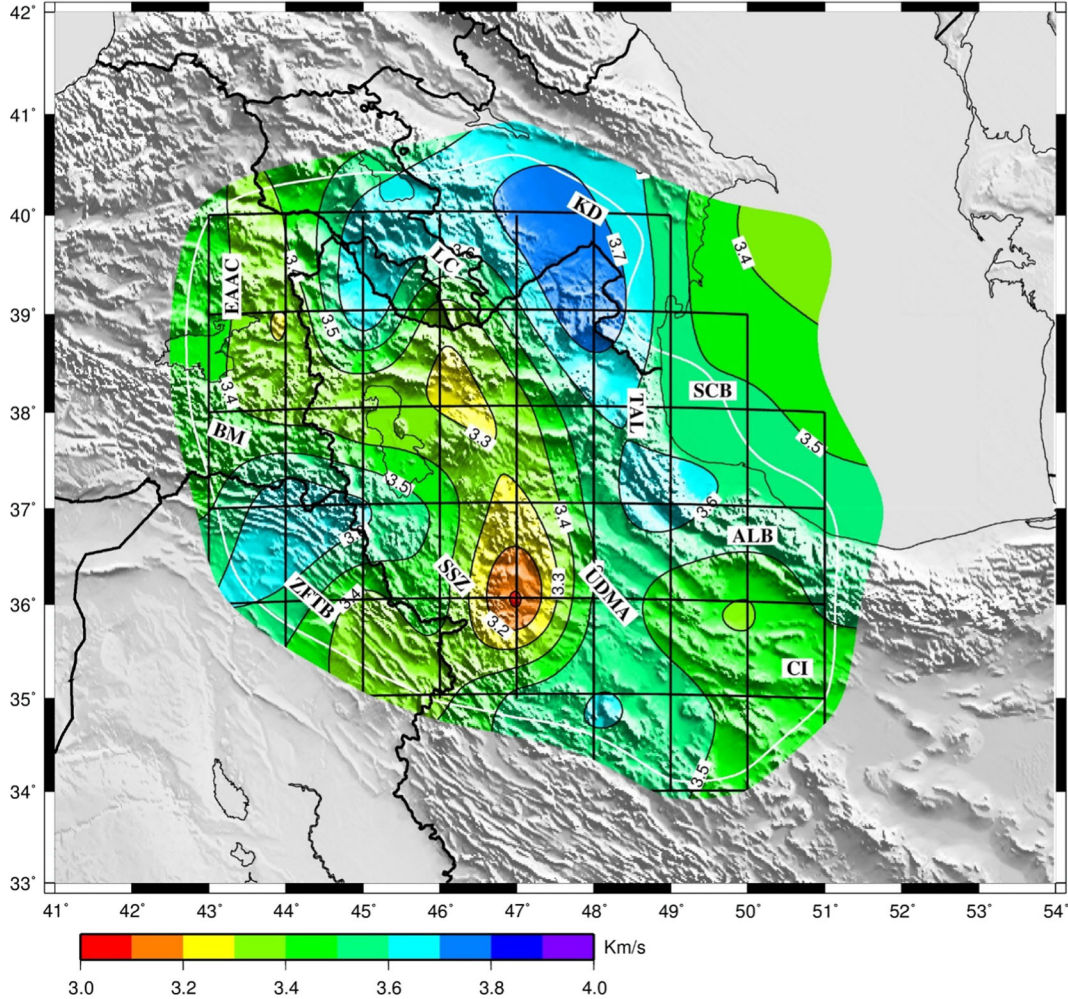
Fig. 9 (continued)

V6 for shear velocity and T1 to T6 for thickness of each layer (Tables 3 and 4). V1 and T1 are fixed parameters while the others are computed. In both minimum RMS and mean velocity models, we present the Moho depth and, when observed, a possible LAB depth. In all the minimum RMS velocity models, we observe a low velocity zone (Fig. 10a–j), probably representing the uppermost asthenosphere layer, while we do not observe such a feature in some of mean velocity models, maybe because of the averaging process. In order to make our following discussions more clear, we have plotted the lateral variations of average V_s of the uppermost 14 km of the crust (Fig. 11), V_s of middle crust (V3 from Table 4, Fig. 12), V_s of lower crust (V4 from Table 4, Fig. 13), and Moho depth (M from Table 4, Fig. 14) using the mean velocity model, and we also plot the lateral variation of the estimated LAB depth from minimum RMS velocity model (L from Table 3, Fig. 15). In the next section, we discuss in more detail the results related to the tomography maps and shear velocity models.

5 Discussion

The Rayleigh wave group velocities in NW Iran and surrounding areas computed from the local and regional events outline within the region different crust and upper

a SCB & KD

b TAL
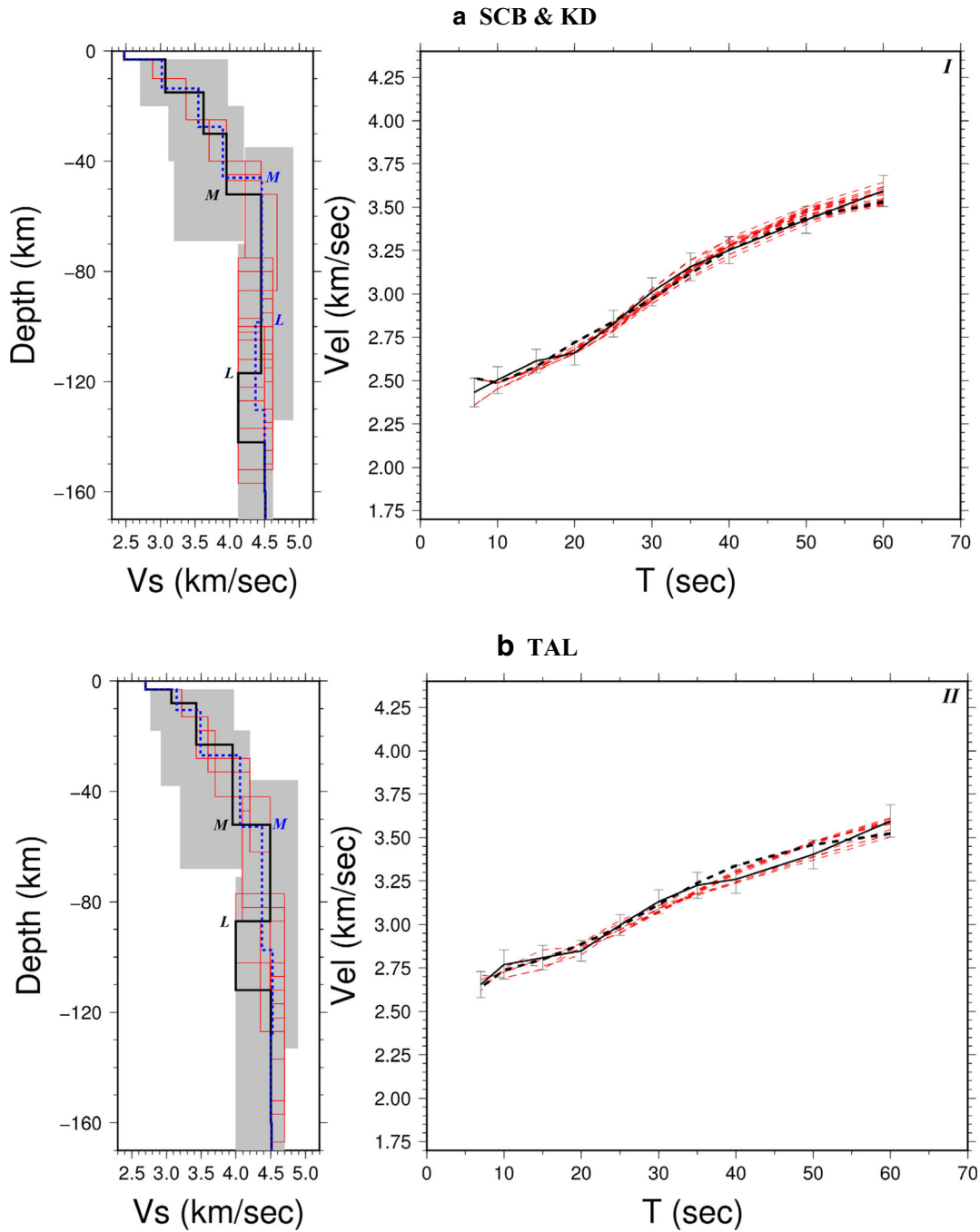
Fig. 10 a–j Left: V_s models corresponding to the average group velocity for the selected tectonic zones in the region. The shaded areas represent the portion of parameter space explored during the inversion, red lines show the all possible solutions, and the black and dashed blue lines represent the solution with minimum RMS and mean of all solutions, respectively. The Black and Blue M and L are the Moho and possible LAB of minimum RMS and mean solution, respectively. Right: the theoretical dispersion curves corresponding to all solutions (dashed red lines), observed average dispersion curve of the tectonic zone (solid black line), the corresponding dispersion curve of the minimum RMS solution (dashed black line) inside the observed error bars. In the top right, the corresponding Latin number of tectonic zone is plotted

19

c NW Iran

d LC
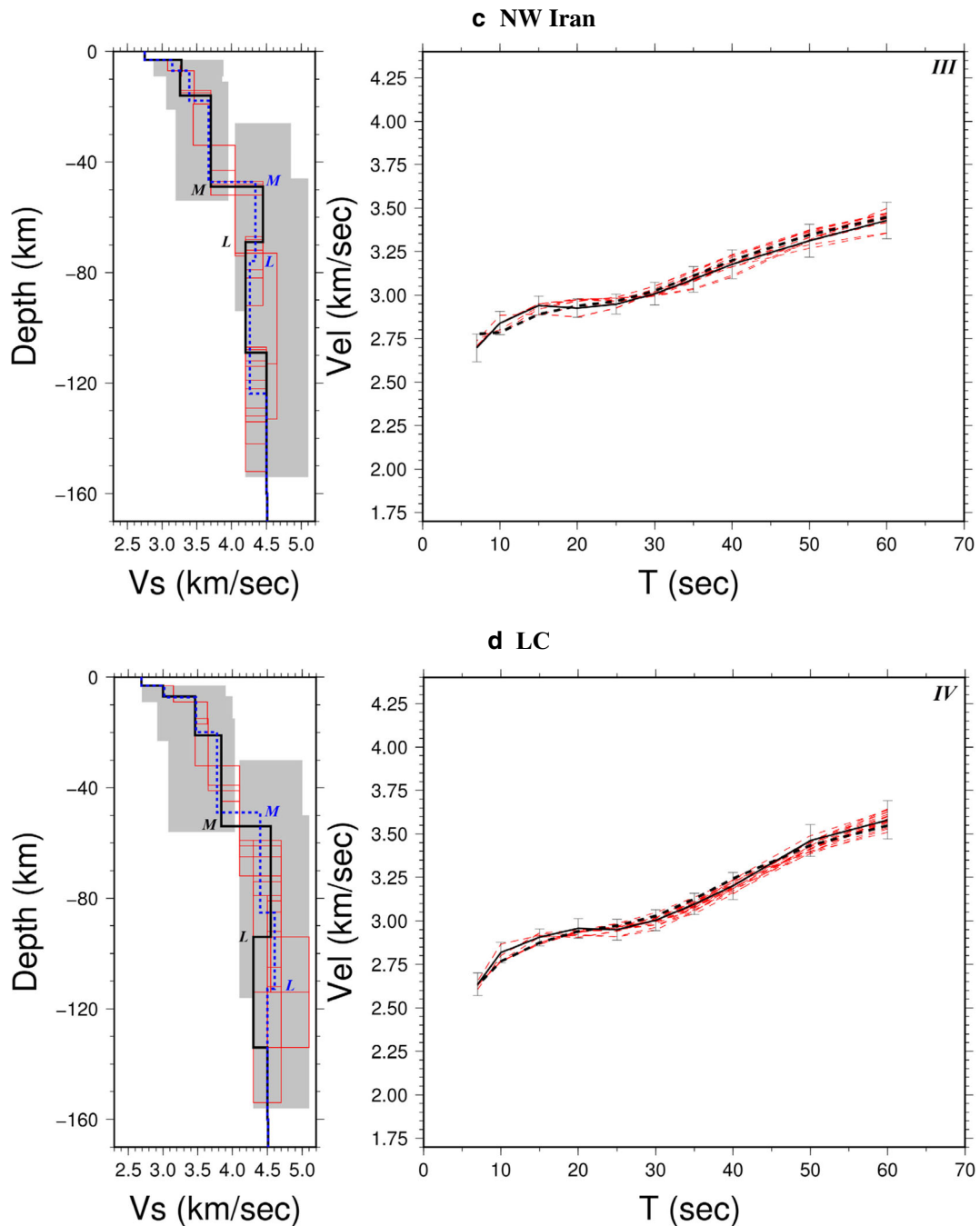
Fig. 10 (continued)

mantle structures that correlate well with the known tectonic features.

The velocities of Rayleigh waves at short periods (7 and 10 s), containing information relative to the upper crust (Fig. 5b), are essentially sensitive to shallow geological features, like sedimentary basins, topography,

and eventually to volcanic features. As the tomographic maps at 7 and 10 s show the same pattern, we just present the tomographic map of 7 s in Fig. 9a (The tomographic map for period of 10 s is shown in Fig. S1 in the electronic supplement), where we observe a relatively high-velocity anomaly along the Alborz,

e EAAC

f BM-SSZ
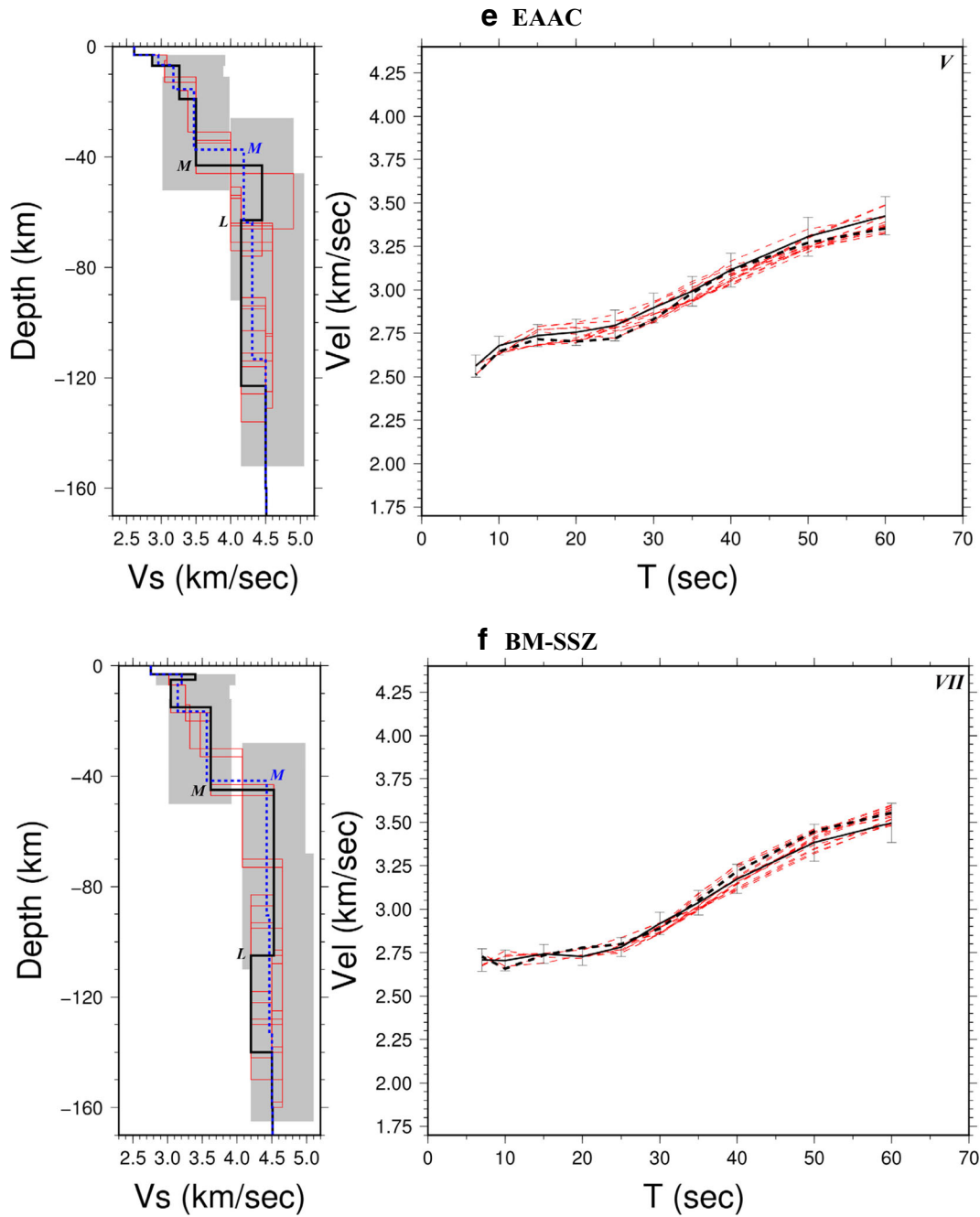
Fig. 10 (continued)

Talesh, and LC, which is bounded by lower velocities in SCB and KD to the east and eastern Anatolia and most of NW Iran to the west. We argue that the lower group velocities in SCB and KD are related to the presence of thick (~14 km) and low-velocity (2.48–3.02 km/s)

sediments that is observed in our depth inversion results (Table 4, Figs. 10 a and 11). On the other side, we think that lower velocities in eastern Anatolia and western parts of NW Iran can be explained by partially melt zones in the crust, in accordance with the study of

g ZFTB

h SSZ
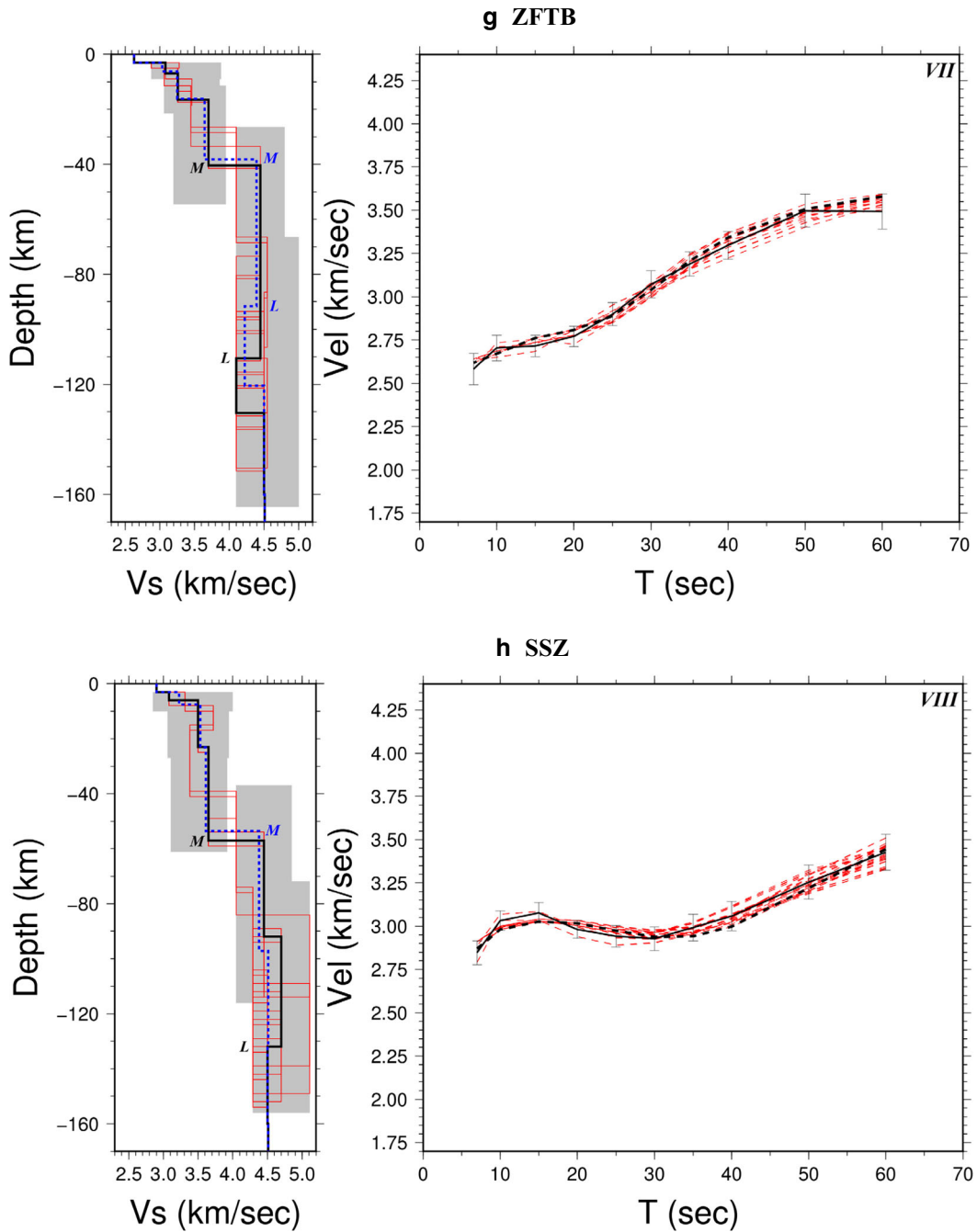
Fig. 10 (continued)

Keskin (2003), who proposed extensive melting in the crust as a result of the interaction of hot asthenosphere with the EAAC. As we expected, we observed low shear velocity in EAAC for the upper part of crust (Tables 3 and 4, Fig. 10e) that is well mapped in Fig. 11 and shows a low velocity zone in EAAC where we have no significant sedimentary basin. In addition, the shallow Curie point depth observed by Aydın et al. (2005), which implies a shallow magma source, is well correlated with the observed low group and shear velocities in eastern

i UDMA and CI

IX

j ALB

X
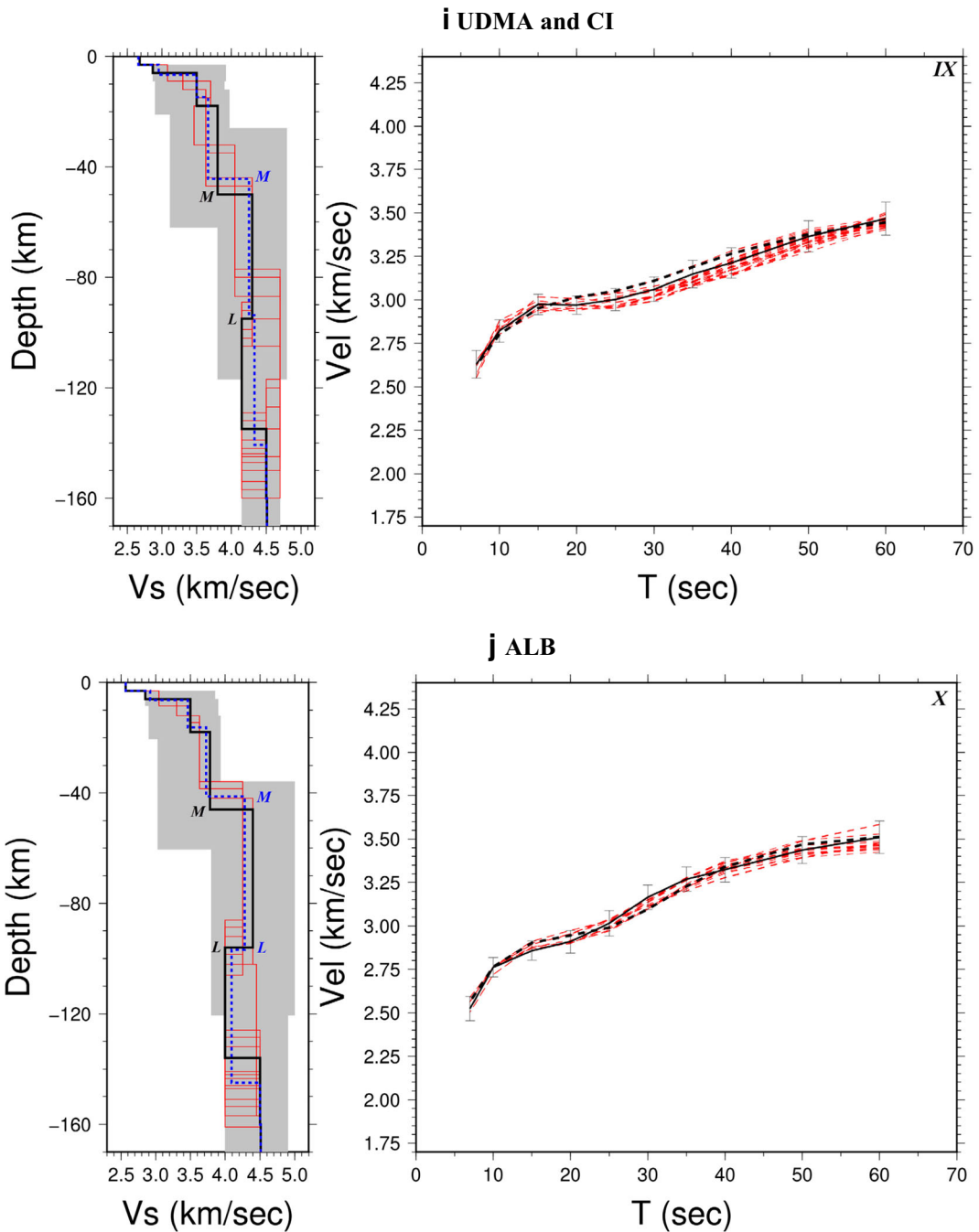
Fig. 10 (continued)

Anatolia; in Lake Urmieh that is a sedimentary basin, we observe as well low velocities.

Another prominent observation is a relatively sharp-contrast high-velocity anomaly along SSZ (Fig. 9a) that is bounded by low-velocity anomalies along UDMA and ZFTB to the east and west, respectively. As we expected, the average V_s of upper crust in Fig. 11 shows the same pattern. Lack of any significant sedimentation and volcanic activities are the main reasons of high shear and group velocities in SSZ. The low group and

Table 3 Minimum RMS V_s model obtained for the selected tectonic zones in the study region

Zone	V1 (km/s)	V2 (km/s)	V3 (km/s)	V4 (km/s)	V5 (km/s)	V6 (km/s)	T1 (km)	T2 (km)	T3 (km)	T4 (km)	T5 (km)	T6 (km)	M (km)	L (km)
SCB and KD (I)	2.48	3.07	3.62	3.95	4.45	4.12	3	12	15	22	65	25	52	117
TAL (II)	2.7	3.07	3.43	3.95	4.49	4.0	3	5	15	29	35	25	52	87
NW Iran (III)	2.75	3.28	3.26	3.7	4.45	4.2	3	4	9	33	20	40	49	69
LC (IV)	2.69	3.0	3.46	3.84	4.55	4.3	3	4	14	33	40	40	54	94
EAAC (V)	2.61	2.87	3.26	3.5	4.45	4.15	3	4	12	24	20	60	43	63
BM-SSZ (VI)	2.76	3.4	3.05	3.62	4.53	4.2	3	2	10	30	60	35	45	105
ZFTB (VII)	2.63	3.08	3.26	3.7	4.45	4.1	3	4	9	24	70	20	40	110
SSZ (VIII)	2.9	3.08	3.5	3.65	4.45	4.7	3	3	17	34	35	40	57	132
UDMA and CI (IX)	2.66	2.87	3.5	3.8	4.3	4.15	3	3	12	32	45	40	50	95
ALB (X)	2.57	2.85	3.5	3.78	4.4	4.0	3	3	12	28	50	40	46	96

Values from V1 to V6 and from T1 to T6 are shear velocities and thicknesses, respectively. V1 and T1 are kept constant during the inversion procedure while V2 to V6 and T2 to T6 are computed. M and L denote Moho and LAB depth, respectively

shear velocities in ZFTB (Figs. 9 a and 11) can be due to weak and cracked upper crust as a result of high-intensity deformation and of the presence of shallow and low-angle thrust and reverse faults (Jackson and Fitch 1981); in UDMA and Central Iran, they can be due to the presence of some local sedimentary basins. The low velocities observed along ZFTB are also well correlated with the high and shallow seismicity in this zone (Maggi et al. 2000; Talebian and Jackson 2004) that implies the presence of an upper crust tectonically very active. Using the Love wave group velocities in the 10–20 s period range, Didem Cambaz and Karabulut

(2010) observed low velocities in EAAC while Pontides to the north and Bitlis–Massif to the south that can be considered as the extension of LC and SSZ into the eastern Anatolia, respectively, display relatively higher velocities, consistently with our results. Didem Cambaz and Karabulut (2010) also found relatively lower velocities uniformly distributed beneath the Arabian platform, in agreement with the relatively lower velocities we measured along ZFTB.

According to the sensitivity kernels shown in Fig. 5b, at 20 s, the Rayleigh wave group velocities are controlled by the upper and lower crust and provide us information about

Table 4 Same as Table 3, for the average V_s model

Zone	V1 (km/s)	V2 (km/s)	V3 (km/s)	V4 (km/s)	V5 (km/s)	V6 (km/s)	T1 (km)	T2 (km)	T3 (km)	T4 (km)	T5 (km)	T6 (km)	M (km)	L (km)
SCB and KD (I)	2.48	3.02	3.55	3.9	4.46	4.37	3	11	14	18	52	32	46	98
TAL (II)	2.7	3.14	3.49	4.06	4.38	4.53	3	7	17	26	44	32	53	*
NW Iran (III)	2.75	3.15	3.39	3.67	4.34	4.26	3	4	11	29	29	48	47	76
LC (IV)	2.69	3.02	3.48	3.78	4.4	4.6	3	4	13	29	36	28	49	113
EAAC (V)	2.61	2.96	3.17	3.47	4.19	4.31	3	4	8	22	27	49	37	*
BM-SSZ (VI)	2.76	3.2	3.15	3.57	4.42	4.46	3	3	11	25	48	44	42	*
ZFTB (VII)	2.63	3.04	3.25	3.64	4.39	4.22	3	3	10	22	54	28	38	92
SSZ (VIII)	2.9	3.23	3.53	3.61	4.38	4.51	3	5	15	31	43	35	54	*
UDMA and CI (IX)	2.66	2.95	3.5	3.66	4.25	4.33	3	4	8	29	50	47	44	*
ALB (X)	2.57	2.92	3.46	3.73	4.28	4.09	3	3	10	25	56	48	41	97

*We did not observe any considerable possible LAB to a depth of 160 km
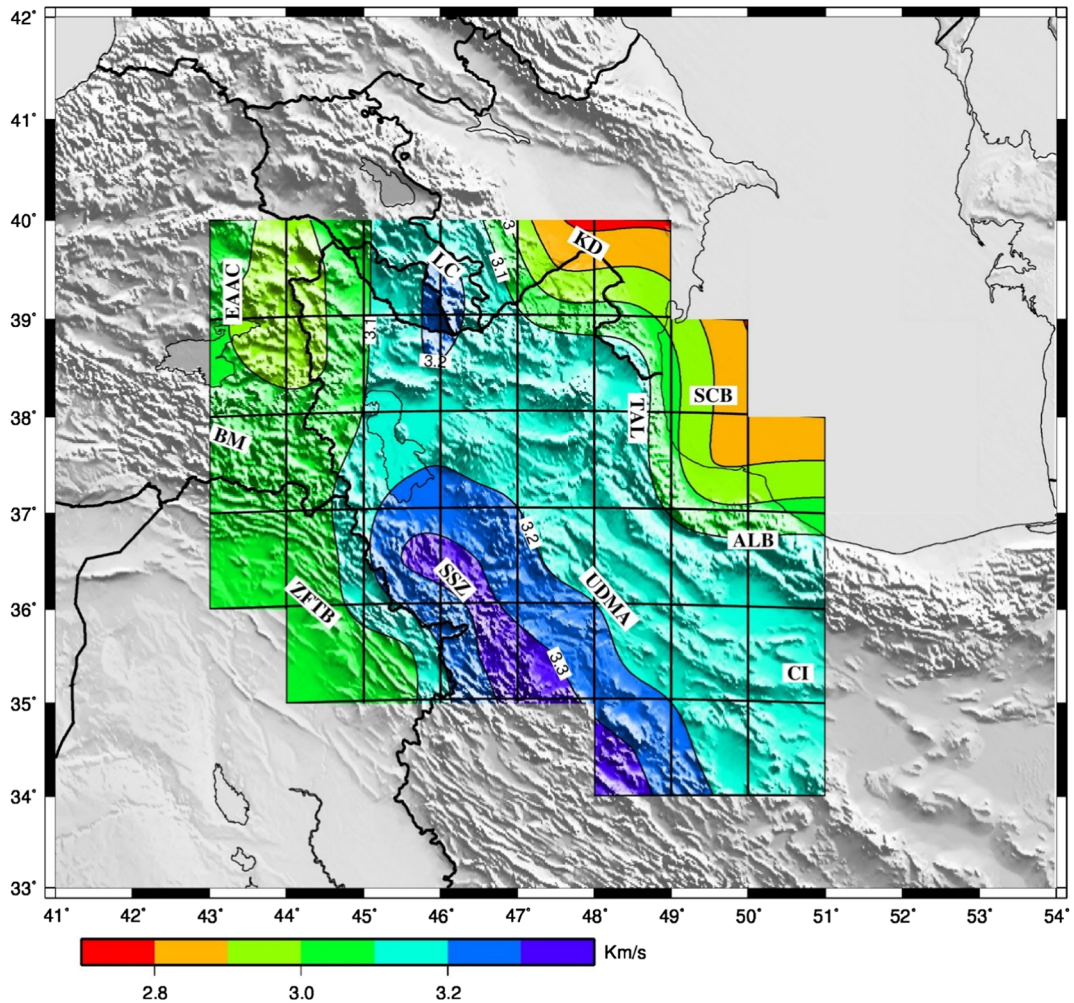
Fig. 11 Average V_s of the uppermost 14 km of the crust from the mean velocity model (Table 4), on shaded topography map. The image is clipped by the boundaries of gridded area. The tomographic cells are plotted using solid black polygons. The main tectonic units are marked

the average crustal structure. The tomographic map at 20 s (Fig. 9b) indicates a uniform distribution of group velocities (< 2.9 km/s) in SCB and KD, consistently with the presence of a similar crustal structure in SCB and KD, which is thought to be an oceanic-like crust, different from the continental crust of NW Iran (Mangino and Priestley 1998). This result is well confirmed by the mapped lateral variations of shear velocity for middle and lower crust (Figs. 12 and 13), where we observe higher shear velocities in SCB and KD relative to NW Iran. The high shear velocity of lower crust in SCB and KD relative to NW Iran (Figs. 13 and 10a, Tables 3 and 4) is also higher than a normal continental crust probably because of its oceanic nature. In most of NW Iran and LC (at latitude > 37°N), except for their western parts, the velocities are approximately the same and show slight variation around ~

2.9 km/s, which outlines a laterally smooth velocity structure of the crust in this region. The maps in Figs. 12 and 13 indicate the same result in NW Iran and LC by lateral variation of shear velocities for middle and lower crust. This result is consistent with the results of Mahri et al. (2016) that performed a 2-D M_L shear velocity tomography for the whole of Iran. The M_L shear velocity is obtained by the division of hypocentral distance to the arrival time of maximum amplitude, used in M_L calculation, and varies between the Sn and Lg velocities. Lg waves are continental low-velocity surface waves produced by combination of higher mode Rayleigh and Love waves (Panza and Calcagnile 1975; Knopoff et al. 1973). In the presence of continental crust with slight Moho depth variation, the M_L velocities are close to Lg velocities, meaning that the region is
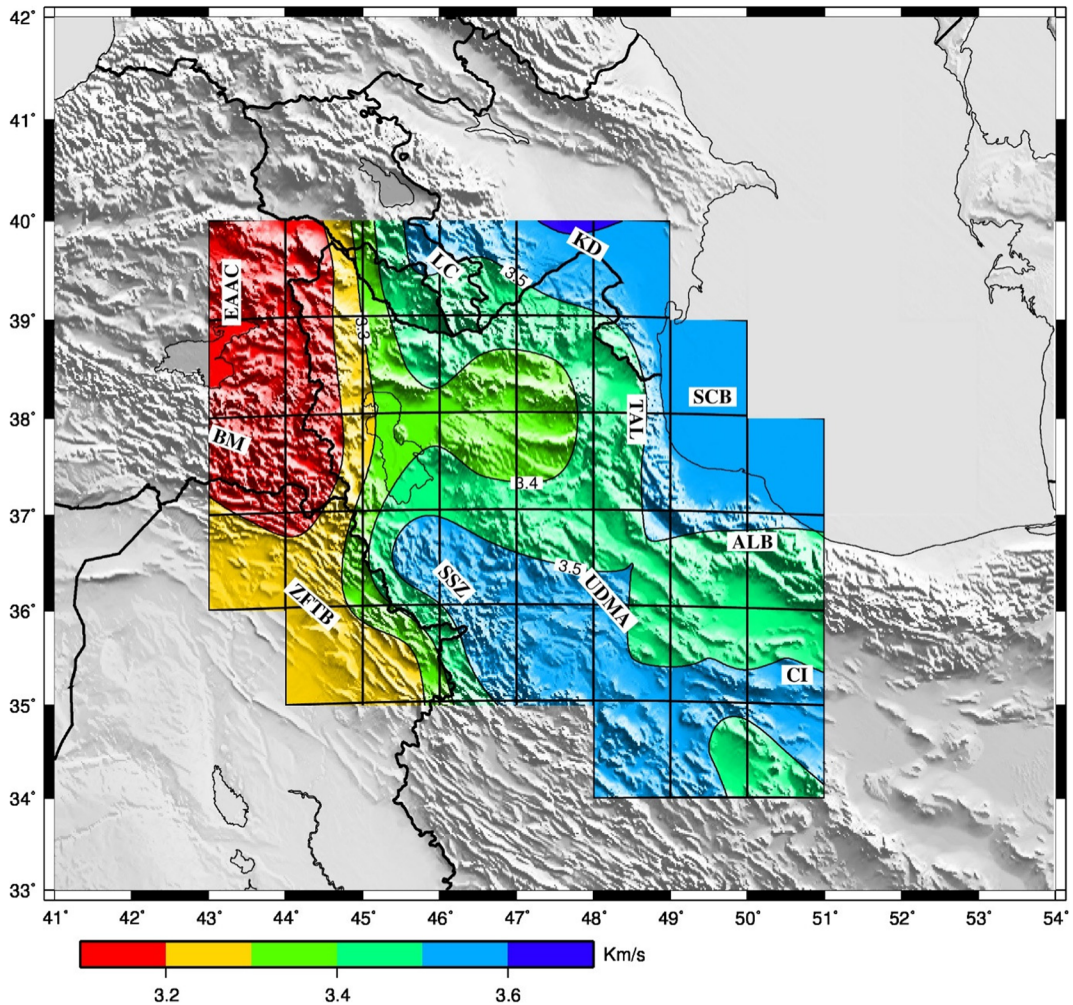
Fig. 12 Same as Fig. 11 for V_s of middle crust (V3 from Table 4)

Lg passing block. Maheri-Peyrov et al. (2016) found that NW Iran has ML velocities in the range of normal Lg waves with slight variations, indicating that this region is Lg-passing and suggesting the presence of smooth Moho undulations and of low shear velocity variations. At latitudes less than 37° N in the western part of ZFTB, the observed low velocities (from ~2.7 to ~2.9 km/s) indicate a different crustal structure with respect to the NW Iran. For the rest of the study area, the result is the same as that obtained in NW Iran, except for SSZ zone where velocities are slightly higher (from ~2.9 to ~3.0 km/s) suggesting the presence of a slightly different crustal structure. The low shear velocities in ZFTB and UDMA in the range of NW Iran and a slightly higher velocities in SSZ is observed in the middle crust and is well correlated with our observations of group velocities (Fig. 12).

Based on both lateral variation of group (Fig. 9b) and shear (Figs. 12 and 13) velocities, we argue that the transition zone from SCB and KD to NW Iran is located below the Alborz, Talesh, and part of the LC, and therefore, the likely oceanic-base crust of SCB seems to extend beneath these mountain ranges. This result is in good agreement with the result of earlier studies like Zanjani et al. (2013), Mortezanejad et al. (2013), and Mangino and Priestley (1998) that identifies a narrow transition zone beneath the Talesh Mountains. A notable observation after comparing the shear velocities of upper, middle, and lower crust of SCB and KD with NW Iran is the lower velocities in upper crust (because of thick sedimentation) and higher velocities in middle and lower crust (because of different origination) of SCB and KD relative to NW Iran. The influencing depth range on Rayleigh dispersion curves at 20 s is in the
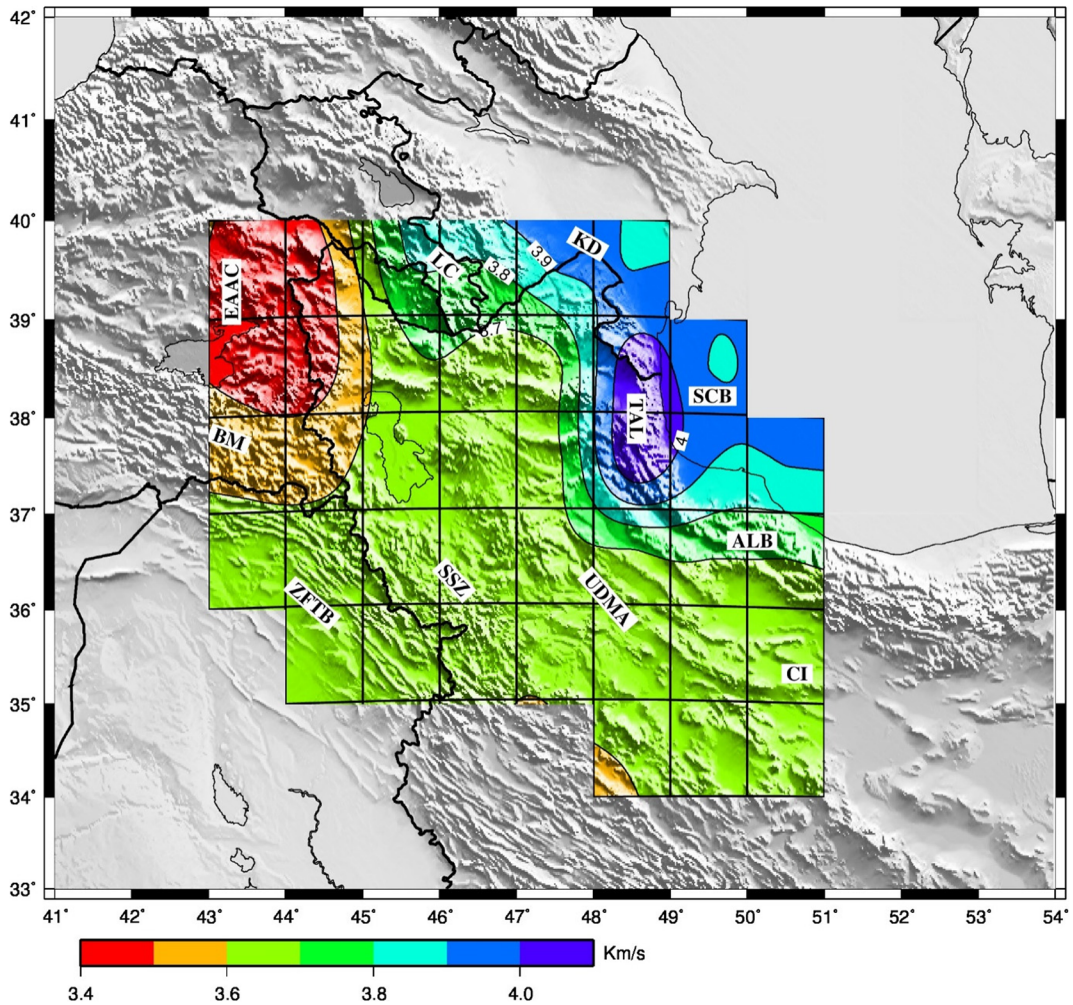
Fig. 13 Same as Fig. 11 for V_s of lower crust (V4 from Table 4)

range of 5 to 35 km (Fig. 5b), which mostly covers the upper and middle crust in SCB and KD (Tables 3 and 4, Fig. 10a), implying that the probable oceanic-base lower crust of SCB and KD has minimum effect on the group velocities at this period while the thick sediments and middle crust have a significant effect. The reason that we observed lower group velocities (< 2.9 km/s) in SCB and KD compared to NW Iran is the higher effect of the low-velocity and thick sediments in upper crust than middle crust on group velocity. The comparison of the shear wave velocity maps of middle and lower crust (Figs. 12 and 13) reveals another characteristic about the transition zone from SCB and KD to NW Iran: in the lower crust, the (high) shear wave velocity of ~ 3.9 km/s in SCB and KD (Table 4, Fig. 10a) further increases to ~ 4.06 km/s beneath Talesh (Table 4, Fig. 10b) while it decreases to ~ 3.73 km/s and ~ 3.78 km/s beneath

Alborz and LC (Table 4, Fig. 10d and j), respectively. In the middle crust, the situation is different: the shear wave velocity of ~ 3.55 km/s in SCB and KD decreases to ~ 3.49, ~ 3.46, and ~ 3.48 beneath Talesh, Alborz, and LC, respectively (Table 4, Fig. 10). This observation indicates that in Talesh, the oceanic-like lower crust of SCB is probably under-thrusting beneath NW Iran while the middle crust is locked. It seems that such under-thrusting is not taking place in the LC and Alborz.

In eastern Anatolia and western part of NW Iran, the group velocities are less than in NW Iran (from ~ 2.6 to ~ 2.9 km/s), with the lowest ones observed in the E and NE of Lake Van. We also observed the same and well-correlated anomalies in the shear velocity maps of middle and lower crust in this tectonic area (Figs. 12 and 13) where we observed the lowest shear velocities within these parts of crust (Tables 3 and 4) in the region of
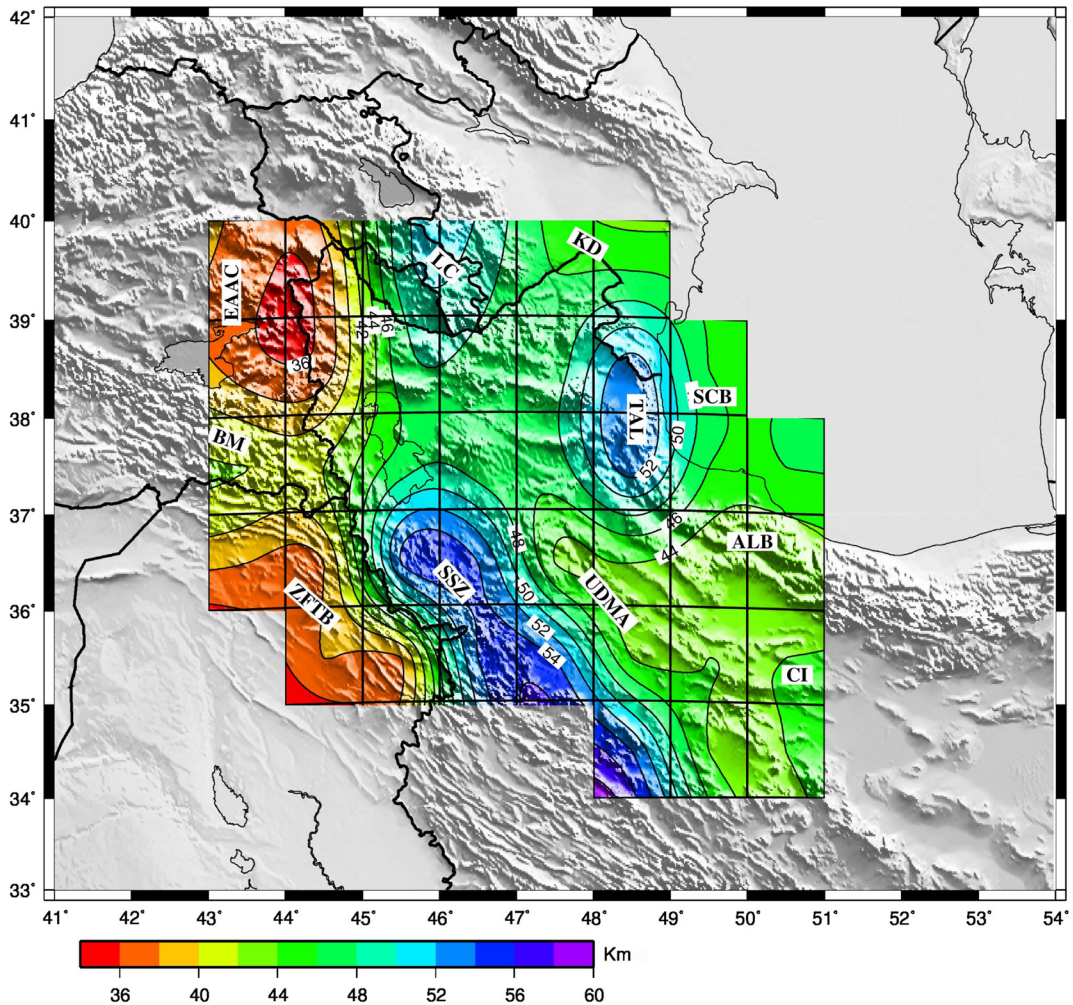
Fig. 14 Same as Fig. 11 for Moho depth from average velocity model (M from Table 4)

study. Like for the shorter periods, we argue that the low velocities in this region can be attributed to partial melting zones inside the crust, as proposed by Keskin (2003).

Rayleigh waves at 35 and 40 s map the velocity structure of the lower crust and uppermost mantle (Fig. 5b); as a result, in continents, low velocities at these periods indicate either the presence of a thick crust overlying a normal continental lid or thin and weak lithospheric mantle beneath a normal crust, while high velocities are usually indicating the presence of a normal continental crust over a stable and thick or oceanic-like lid. Since the pattern in the tomographic maps at 35 and 40 s is similar, we just present here the tomographic map at 40 s in Fig. 9c (The tomographic map for period of 35 s is shown in Fig. S2 in the electronic supplement). In our case, the map shows relatively low velocities in

most of the study area, except in some parts of LC and Alborz, on one side and ZFTB on the other side (Fig. 9c). According to several studies (e.g., Keskin 2003), the mantle lid is thin or absent in the region and we conclude that low velocities in most of the region are related to the presence of such thin continental lithospheric mantle that is well observed in the depth inversion results for NW Iran and EAAC (Fig. 10c, e) where we found LAB at depth of 63 and 69 km (Table 3, Fig. 15), respectively.

In three local areas, one in EAAC and two along the SSZ and Talesh mountains, labeled with L1, L2, and L3 in Fig. 9c, low-velocity anomalies are observed at 40 s. L1 is located east and northeast of Lake Van and just south of four major volcanoes (Ararat, Tendurk, Girekol, and Suphan in Fig. 1) in the region. According to the result of Zor et al.

28
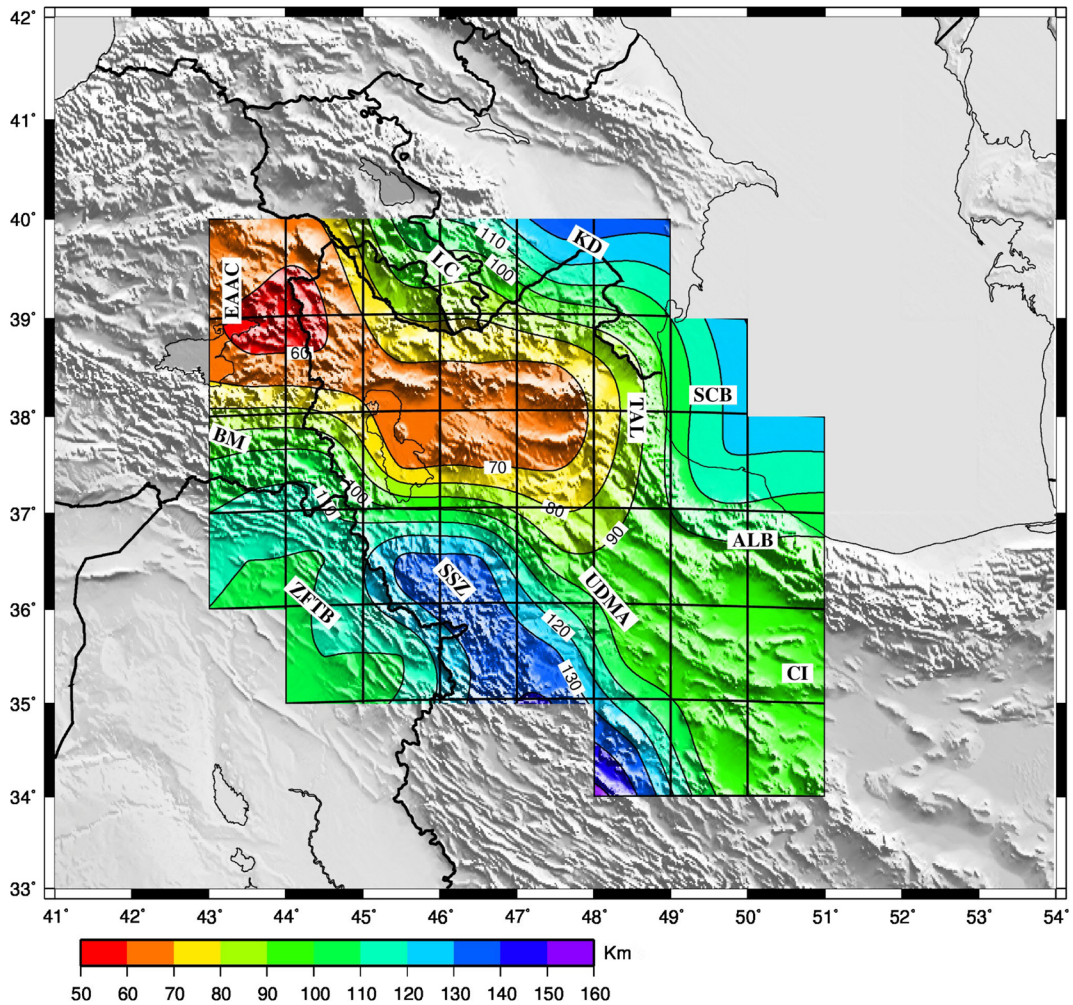
Fig. 15 Same as Fig. 11 for LAB depth from minimum RMS velocity model (L from Table 3)

(2003), the Moho depth decreases south-eastward in eastern Anatolia, especially beneath L1. Considering the similar low-velocity anomalies at shorter periods (≤ 20 s) in L1, and the result of Zor et al. (2003), we argue that the anomaly beneath L1 marks a LAB shallower than in the rest of the region, with the lowest LAB depth located as the minimum velocity in the L1 anomaly (Fig. 9c). The obtained LAB depth of 63 km in our inversion results, which is the lowest value in the study region (Table 3, Figs. 10 e and 15), confirms such interpretation.

Crossing Zagros from SW to NE, the velocities in SSZ decrease. This trend is observed throughout the Zagros Mountains. Based on the high-velocity anomalies along the SSZ at shorter periods (≤ 20 s) and on the result of Paul et al. (2006, 2010), implying thickening of crust along this zone, this fact can be explained by a

possible crustal thickening beneath the region as a result of Arabian–Eurasian collision. Our shear velocity models strongly confirm such crustal thickening (Tables 3 and 4, Figs. 10 g–i and 14) along the SSZ since, based on mean velocity models, the 38 km Moho depth in ZFTB increases to 54 km in SSZ and then decreases to 44 km in UDMA and CI (Fig. 14). With the same logic, we conclude that the low-velocity anomaly beneath L2 is related to a thicker crust in SSZ, where the thickest crustal depth might be located in the position of the minimum velocity at the L2 anomaly (Fig. 9c). We do not observe such crustal thickening in the extension of SSZ toward BM metamorphic zone (Tables 3 and 4 and Fig. 10f).

We relate the L3 low velocity anomaly beneath Talesh to the narrow thickening of the crust that is well resolved by Mortezanejad et al. (2013). The

lateral variation of Moho depth in Fig. 14 confirms such local crustal thickening in Talesh, where, based on mean velocity models, the Moho depth of 53 km is deeper than those value of 46 and 47 km in SCB and NW Iran (Table 4, Fig. 10a–c), respectively; this relative thickening is also observed in LC but not in Alborz (Tables 3 and 4, Figs. 10 d, j and 14).

A remarkable observation about EAAC is that the Lowest Moho depth (37 km, based on mean velocity model, Table 4) in the region is observed in this tectonic zone, where we also observed the lowest LAB depth beside the lowest shear velocities within the crust. We argue that such observation is the result of thinning of mantle lid in the region (based on the result of mean velocity model, Table 4) or of the absence of mantle lid (based on the result of minimum RMS velocity model, Table 3).

In Fig. 9c, a high-velocity zone is also observed in Alborz, west and south of Talesh, and most of LC on one side and ZFTB on the other side. However, due to the local sparse ray coverage, the anomalies beneath ZFTB are not well resolved. We tentatively relate this observation to a different lithospheric structure beneath these regions when compared to that of NW Iran. The thin lithosphere of NW Iran and EAAC (69 and 63 km from Table 3, respectively), which becomes thicker to the east beneath SCB to a value of 117 km and to the SW to the value of 132 and 110 km beneath SSZ and ZFTB, respectively (Table 3, Figs. 10a, g, h and 15), confirms such interpretation.

The Rayleigh waves at 55 and 60 s are more influenced by the velocity structure of the uppermost mantle and at these periods the low-velocity anomalies are mainly due to a thin lithosphere or to the absence of lithospheric mantle, while high velocities can be related to the presence of a stable continental mantle lid or of an oceanic-like lithosphere. Since the pattern in the tomographic maps at 55 and 60 s is similar, we just present here the map of 60 s in Fig. 9d while the map of 55 s is shown in Fig. S3 in the electronic supplement. The tomographic maps at 60 s we obtained reveal low velocities in most of the study area, which is bounded by high-velocity zones in LC, Talesh, Alborz, and SCB on one side and in ZFTB on the other side (Fig. 9d). The explanation can be similar to the one given for period of 40 s, with the emphasis on the possible presence of a thin mantle lid or absence of lithospheric mantle. The lateral variation of LAB depth in Fig. 15 confirms such interpretation.

Like at shorter periods, the lowest group velocities are observed beneath L1 and L2 in the EAAC and along the SSZ consistently with a strong effect of the shallow LAB in eastern Anatolia and the quite thick crust in SSZ.

We explain the high-velocity anomalies beneath LC, Talesh, Alborz, SCB, and ZFTB with the observed high thicker LAB depth beneath these regions (Table 3, Fig. 15). This result is consistent with the result of several earlier studies (e.g., Mangino and Priestley 1998) that indicate the presence of a thick high-velocity mantle lid under Zagros and South Caspian Sea.

Our results also show a strong correlation with those of a recent study by Bavali et al. (2016), who investigated the crust and upper mantle structure of NW Iran and SCB using teleseismic body wave tomography. They observed a high-velocity region that extends to a depth of about 100 km in the SCB thus implying that the lithospheric structure between the NW Iran and SCB is different and LAB is deeper than 100 km in SCB. Based on high velocities in the uppermost mantle, they suggested an oceanic nature for the South Caspian lithosphere.

The high-velocity anomaly observed in the South Caspian Sea extends beneath Talesh, Alborz, and LC (Fig. 9d) and indicates the extension of the South Caspian Sea lithosphere beneath these mountain ranges. This result is in agreement with a limited underthrusting of the SCB beneath Talesh as indicated by Bavali et al. (2016) and Mangino and Priestley (1998). The mapped lateral variation of LAB derived from minimum RMS velocity models is an evidence confirming such extension (Fig. 15).

6 Conclusions

From the analysis of the surface wave tomographic study and shear velocity depth inversions discussed in this paper, we conclude that the mantle lid is thin in NW Iran and EAAC, while in the SCB, Talesh, and LC on one side and ZFTB and SSZ on the other side, it is thick. On average, the thinnest mantle lid of 63 km is observed beneath EAAC where we observed a low group velocity anomaly not only at long periods (≥ 35 s) consistently with a thin or absent mantle lid, but also at periods shorter than 20 s. This fact indicate that the anomaly is not limited to the

upper mantle but that it extends into the lower crust where we observed lower shear velocities within the crust in the region of study. The main process of such intrusion, whose amount is reduced toward NW Iran, could be related to the existence of partial melting zones inside the crust. The point labeled L1 in EEAC and located at east and northeast of Lake Vane (Fig. 9c) have probably the shallowest LAB depth in the study area.

In Zagros, namely in SSZ, high- and low-velocity anomalies are seen at short ($T \leq 20$ s) and long ($T \geq 35$ s) periods, respectively, and they were interpreted as relative thickening of the crust along SSZ, demonstrated by shear velocity models obtained for this tectonic area. The location with the possible thickest crust in the study area is labeled L2 in Fig. 9c. The crust and upper mantle structure in ZFTB and UDMA is different when compared to that of the SSZ. Both Moho and LAB depths increase beneath SSZ when crossing the Zagros range from ZFTB to UDMA.

In the South Caspian Sea, there is a significant difference in both crustal and upper mantle structure relative to NW Iran. The crust and upper mantle structure is similar in the South Caspian Sea and KD and both features extend beneath Talesh, Alborz, and LC. In Talesh, an under-thrusting of the lower crust of SCB beneath NW Iran is observed, while the middle crust is locked. This under-thrusting is not taking place in Alborz and LC. The observed 14-km-thick sediment cover in SCB is well compatible with our results that indicate low group velocity anomalies at short ($T \leq 10$ s) periods. The high shear velocity in the lower crust of SCB relative to NW Iran is probably because of the oceanic source of the lower crust in this region. A localized relative thickening of the crust to a depth of 53 km beneath Talesh Mountains is observed only between South Caspian Sea and NW Iran.

References

Agard P, Omrani J, Jolivet L, Whitechurch H, Vrielynck B, Spakman W, Monie P, Meyer B, Wortel R (2011) Zagros orogeny: a subduction-dominated process. Geol Mag 148(5–6):692–725

Alavi M (1994) Tectonics of the Zagros orogenic belt of Iran: new data and interpretation. Tectonophysics 229:211–238

Al-Lazki AI, Seber D, Sandvol E, Turkelli N, Mohamad R, Barazangi M, (2003) Tomographic Pn velocity and anisotropy structure beneath the Anatolian plateau (eastern Turkey) and the surrounding regions. Geophys Res Lett 30(24). https://doi.org/10.1029/2003GL017391

Al-Lazki AI, Sandvol E, Seber D, Barazangi M, Turkelli N, Mohamad R (2004) Pn tomographic imaging of mantle lid velocity and anisotropy at the junction of the Arabian, Eurasian and African plates. Geophys J Int 158:1024–1040

Al-Lazki AI, Al-Damegh KS, El-Hadidy SY, Ghods A, Tatar M (2014) Pn velocity structure beneath Arabia–Eurasia Zagros collision and Makran subduction zones. Geol Soc Lond, Spec Publ 392(1):45–60

Asudeh I (1982) Seismic structure of Iran from surface and body wave data. Geophys J R Astron Soc 71:715–730

Aydın I, Karat HI, Kocak A (2005) Curie-point depth map of Turkey. Geophys J Int 162:633–640

Bavali K, Motaghi K, Sobouti F, Ghods A, Abbasi M, Priestley K, Mortezanejad G, Rezaeian M (2016) Lithospheric structure beneath NW Iran using regional and teleseismic travel-time tomography. Phys Earth Planet Inter 253:97–107. https://doi.org/10.1016/j.pepi.2016.02.006

Brunet MF, Korotaev MV, Ershov AV, Nikishin AM (2003) The South Caspian Basin: a review of its evolution from subsidence modelling. Sediment Geol 156:119–148

Chiu HY, Chung SL, Zarrinkoub MH, Mohammadi SS, Khatib MM, Iizuka Y (2013) Zircon U–Pb age constraints from Iran on the magmatic evolution related to Neotethyan subduction and Zagros orogeny. Lithos 162–163:70–87

Dehghani GA, Makris J (1984) The gravity field and crustal structure of Iran. Neues Jahrb Geol Palaontol Abh 168:215–229

Didem Cambaz M, Karabulut H (2010) Love-wave group velocity maps of Turkey and surrounding regions. Geophys J Int 181:502–520. https://doi.org/10.1111/j.1365-246X.2010.04516.x

Ditmar PG, Yanovskaya TB (1987) A generalization of the Backus–Gilbert method for estimation of lateral variations of surface wave velocity. Izv Phys Solid Earth, 23 (6), 470–477

Giese P, Makris J, Akashe B, Rower P, Letz H, Mostaanpour M (1984) The crustal structure in southern Iran derived from seismic explosion data. Neues Jahrb Geol Palaontol Abh 168:230–243

Gok R, Pasyanos ME, Zor E (2007) Lithospheric structure of the continent–continent collision zone: eastern Turkey. Geophys J Int 169(3):1079–1088

Herrmann RB, Ammon CJ, (2004) Surface waves, receiver functions and crustal structure, in Computer Programs in Seismology. Version 3.30, Saint Louis University, http://www.eas.slu.edu/People/RBHerrmann/CPS330.html

Hessami K, Jamali F, Tabassi H (2003) Major active faults of Iran, edition 2003. International Institute of Earthquake Engineering and Seismology, Tehran

Jackson JA, Fitch T (1981) Basement faulting and the focal depths of the larger earthquakes in the Zagros Mountains (Iran). Geophys J R Astron Soc 64:561–586

Jackson JA, Priestley K, Allen M, Berberian M (2002) Active tectonics of the South Caspian Basin. Geophys J Int 148(2):214–245

Karagianni EE, Panagiotopoulos DG, Panza GF, Suhadolc P, Papazachos CB, Papazachos BC, Kiratzi A, Hatzfeld D, Makropoulos K, Priestley K, Vuan A (2002) Rayleigh wave group velocity tomography in the Aegean area. Tectonophysics 358:187–209

Keskin M (2003) Magma generation by slab steepening and breakoff beneath a subduction accretion complex: an alternative model for collision-related volcanism in eastern Anatolia, Turkey. Geophys Res Lett 30(24). https://doi.org/10.1029/2003GL018019

Keskin M, Pearce JA, Mitchell JG (1998) Volcano-stratigraphy and geochemistry of collision-related volcanism on the Erzurum–Kars plateau, north eastern Turkey. J Volcanol Geotherm Res 85:355–404

Knapp JH, Connor JA (2004) Crustal-scale structure of the South Caspian Basin revealed by deep seismic reflection profiling. Mar Pet Geol 21:1073–1081

Knopoff L, Schwab F, Kausel E (1973) Interpretation of Lg. Geophys J R Astron Soc 33:389–404

Levshin AL, Ratnikova LI, Berteussen KA (1972) On a frequency–time analysis of oscillations. Ann Geophys 28:211–218

Levshin AL, Ratnikova LI, Berger J (1992) Peculiarities of surface wave propagation across Central Eurasia. Bull Seismol Soc Am 82:2464–2493

Maggi A, Priestley K (2005) Surface waveform tomography of the Turkish Iranian plateau. Geophys J Int 160:1068–1080

Maggi A, Jackson JA, Priestley K, Baker C (2000) A re-assessment of focal depth distributions in southern Iran, the Tien Shan and northern India: do earthquakes really occur in the continental mantle? Geophys J Int 143:629–661

Maheri-Peyrov M, Ghods A, Abbasi M, Bergman E, Sobouti F (2016) M_L shear wave velocity tomography for the Iranian plateau. Geophys J Int 205:179–191. https://doi.org/10.1093/gji/ggv504

Mangino S, Priestley K (1998) The crustal structure of the southern Caspian region. Geophys J Int 133:630–648

Mortezanejad G, Aziz Zanjani A, Ghods A, Sobouti F (2013) Insights into the crustal structure and the seismotectonics of the Talesh region using the local and teleseismic data. Geosciences 88(2):38–47

Panza GF (1981) The resolving power of seismic surface waves with respect to crust and upper mantle structural models. In: The solution of the inverse problem in geophysical interpretation, Ed.: Cassinis, R., Plenum Pub. Corp., 39–77

Panza GF, Calcagnile G (1975) Lg, Li and Rg from Rayleigh modes. Geophys J R Astron Soc 40:475–487

Paul A, Kaviani A, Hatzfeld D, Vergne J, Mokhtari M (2006) Seismological evidence for crustal-scale thrusting in the Zagros mountain belt (Iran). Geophys J Int 166:227–237

Paul A, Hatzfeld D, Kaviani A, Tatar M, Pequegnat C (2010) Seismic imaging of the lithospheric structure of the Zagros mountain belt (Iran). Geol Soc Lond Spec Publ 330:5–18

Priestley K, McKenzie D, Barron J, Tatar M, Debayle E (2012) The Zagros core: deformation of the continental lithospheric mantle. Geochem Geophys Geosyst 13:Q11014

Raykova RB, Panza GF (2010) The shear-wave velocity structure of the lithosphere–asthenosphere system in the Iberian area and surroundings. Rend Fis Acc Lincei 21:183–231. https://doi.org/10.1007/s12210-010-0077-1

Ritzwoller MH, Shapiro NM, Barmin MP, Levshin AL (2002) Global surface wave diffraction tomography. J Geophys Res 107:2335. https://doi.org/10.1029/2002JB001777

Sengor AMC (1990) A New Model for the Late Palaeozoic-Mesozoic Tectonic Evolution of Iran and Implications for Oman, In: Robertson, A.H.F., Searle, M.P. and Ries, A.C., Eds., The Geology and Tectonics of the Oman Region. Geol Soc Spec Publ 49:797–831.

Sengor AMC, Ozeren S, Zor E, Genc T (2003) East Anatolian high plateau as a mantle-supported, N–S shortened domal structure. Geophys Res Lett 30(24):8045. https://doi.org/10.1029/2003GL017858

Stocklin J (1968) Structural history and tectonics of Iran: a review. Am Assoc Pet Geol Bull 52:1229–1258

Taghizadeh-Farahmand F, Sodoudi F, Afsari N, Ghassemi MR (2010) Lithospheric structure of NW Iran from P and S receiver functions. J Seismol 14(4):823–836

Talebian M, Jackson JA (2002) Offset on the main recent fault of the NW Iran and implications for the Late Cenozoic tectonics of the Arabia–Eurasia collision zone. Geophys J Int 150:422–439

Talebian M, Jackson JA (2004) A reappraisal of earthquake focal mechanisms and active shortening in the Zagros mountains of Iran. Geophys J Int 156:506–526

Urban L, Cichowicz A, Vaccari F (1993) Computation of analytical partial derivatives of phase and group velocities for Rayleigh waves with respect to structural parameters. Stud Geophys Geod 37:14–36

Yanovskaya TB (1997) Resolution estimation in the problems of seismic ray tomography. Izv Phys Solid Earth 33(9):762–765

Yanovskaya TB, Kizima ES, Antomova LM (1998) Structure of the crust in the Black Sea and adjoining regions from surface wave data. J Seismol 2:303–316

Yilmaz Y (1990) Comparison of young volcanic associations of western and eastern Anatolia formed under a compressional regime: a review. J Volcanol Geotherm Res 44:69–87

Zanjani AA, Ghods A, Sobouti F, Bergman E, Mortezanejad G, Priestley K, Madanipour S, Rezaeian M (2013) Seismicity in the western coast of the South Caspian Basin and the Talesh Mountains. Geophys J Int 195(2):799–814

Zor E, Sandvol E, Gorbuz C, Turkelli N, Seber D, Barazangi M (2003) The crustal structure of the east Anatolian plateau (Turkey) from receiver functions. Geophys Res Lett 30(24):8044. https://doi.org/10.1029/2003GL018192